Quaternary Research (2022), **105**, 201–217
doi:10.1017/qua.2021.42

Research Article

Holocene geo-ecological evolution of Lower Geyser Basin, Yellowstone National Park (USA)

Christopher M. Schiller[a]*, Cathy Whitlock[a,b] and Sabrina R. Brown[c]

[a]Department of Earth Sciences, Montana State University, Bozeman, MT 59717, USA; [b]Montana Institute on Ecosystems, Montana State University, Bozeman, MT 59717, USA and [c]Environmental Science Program, Defiance College, Defiance, OH 43512, USA

Abstract

Changes in climate and fire regime have long been recognized as drivers of the postglacial vegetation history of Yellowstone National Park, but the effects of locally dramatic hydrothermal activity are poorly known. Multi-proxy records from Goose Lake have been used to describe the history of Lower Geyser Basin where modern hydrothermal activity is widespread. From 10,300 cal yr BP to 3800 cal yr BP, thermal waters discharged into the lake, as evidenced by the deposition of arsenic-rich sediment, fluorite mud, and relatively high $\delta^{13}C_{sediment}$ values. Partially thermal conditions affected the limnobiotic composition, but prevailing climate, fire regime, and rhyolitic substrate maintained *Pinus contorta* forest in the basin, as found throughout the region. At 3800 cal yr BP, thermal water discharge into Goose Lake ceased, as evidenced by a shift in sediment geochemistry and limnobiota. Pollen and charcoal data indicate concurrent grassland development with limited fuel biomass and less fire activity, despite late Holocene climate conditions that were conducive to expanded forest cover. The shift in hydrothermal activity at Goose Lake and establishment of the treeless geyser basin may have been the result of a tectonic event or change in hydroclimate. This record illustrates the complex interactions of geology and climate that govern the development of an active hydrothermal geo-ecosystem.

Keywords: Vegetation history, Fire history, Pollen, Charcoal, Diatoms, Hydrothermal activity, Lodgepole pine

(Received 5 March 2021; accepted 15 June 2021)

INTRODUCTION

The Yellowstone Plateau Volcanic Field hosts one of the largest and most diverse continental hydrothermal systems on Earth (Hurwitz and Lowenstern, 2014). More than 10,000 thermal features are found in the volcanic field, concentrated within the Yellowstone caldera (http://rcn.montana.edu/Features/Search.aspx, accessed July 2020). Thermal areas occupy more than 48 km^2 in Yellowstone National Park (Vaughan et al., 2014) and present-day thermal areas have been active since at least late glacial time (Muffler et al., 1971, 1982; Fournier, 1989; Sturchio et al., 1994; Pierce et al., 2007a).

The influence of hydrothermal activity on Yellowstone's terrestrial and limnologic ecosystems is poorly known but seems to occur on many time scales. At present, for example, shifts in the flow of hot, mineral-saturated fluids lead to plant mortality (Channing and Edwards, 2003), and heated soils change vegetation communities and stunt tree growth (Miller, 1968; Pitt and Hutchinson, 1982; White et al., 1988; Lowenstern et al., 2003). On decadal time scales, a newer study finds that a persistent drought during the Medieval Climate Anomaly led to a shutdown of Old Faithful eruptions for several decades in the early thirteenth to middle fourteenth century, allowing conifers to encroach on the geyser mound itself (Hurwitz et al., 2020). In postglacial time, paleoecological data suggest rapid but temporary damage to past vegetation from large hydrothermal explosions in Yellowstone Lake (Schiller et al., 2020), and both short-lived and persistent effects, potentially driven by transformed benthic substrate, to diatom communities (Brown, 2019). Despite these examples, we have little understanding of the long-term ecological consequences of shifting hydrothermal activity in an active thermal basin, nor are we able to evaluate the relative importance of geology and climate in shaping the ecological history of these settings.

Here, we focus on the geo-ecological history of Lower Geyser Basin (LGB), the largest thermal area in Yellowstone National Park (topographic area ~25 km^2, active thermal area ~14 km^2) (Fig. 1B; Vaughan et al., 2014). A series of small lakes lies within LGB in close proximity to active thermal features. This juxtaposition enables use of lake sediment records to examine the interaction between past hydrothermal activity, climate, and ecosystem responses. An 808.5 cm-long sediment core from the largest of the LGB lakes, Goose Lake (44.54°N, 110.84°W, 2196 m asl, 13.8 ha, Fig. 1C), was studied to address the following questions: (1) What is the history of hydrothermal activity at and near Goose Lake as registered in the lake sediment archive? (2) What was the role of climate, hydrothermal activity, and fire in shaping the LGB geo-ecosystem, including its Holocene vegetation and limnologic history relative to other parts of the Yellowstone Plateau?

SITE DESCRIPTION

Situated within the 630 ka Yellowstone caldera, Lower Geyser Basin (LGB) is a large, predominantly treeless basin (Fig. 1B),

*Corresponding author e-mail address: christopherschiller@montana.edu

Cite this article: Schiller CM, Whitlock C, Brown SR (2022). Holocene geo-ecological evolution of Lower Geyser Basin, Yellowstone National Park (USA). *Quaternary Research* **105**, 201–217. https://doi.org/10.1017/qua.2021.42

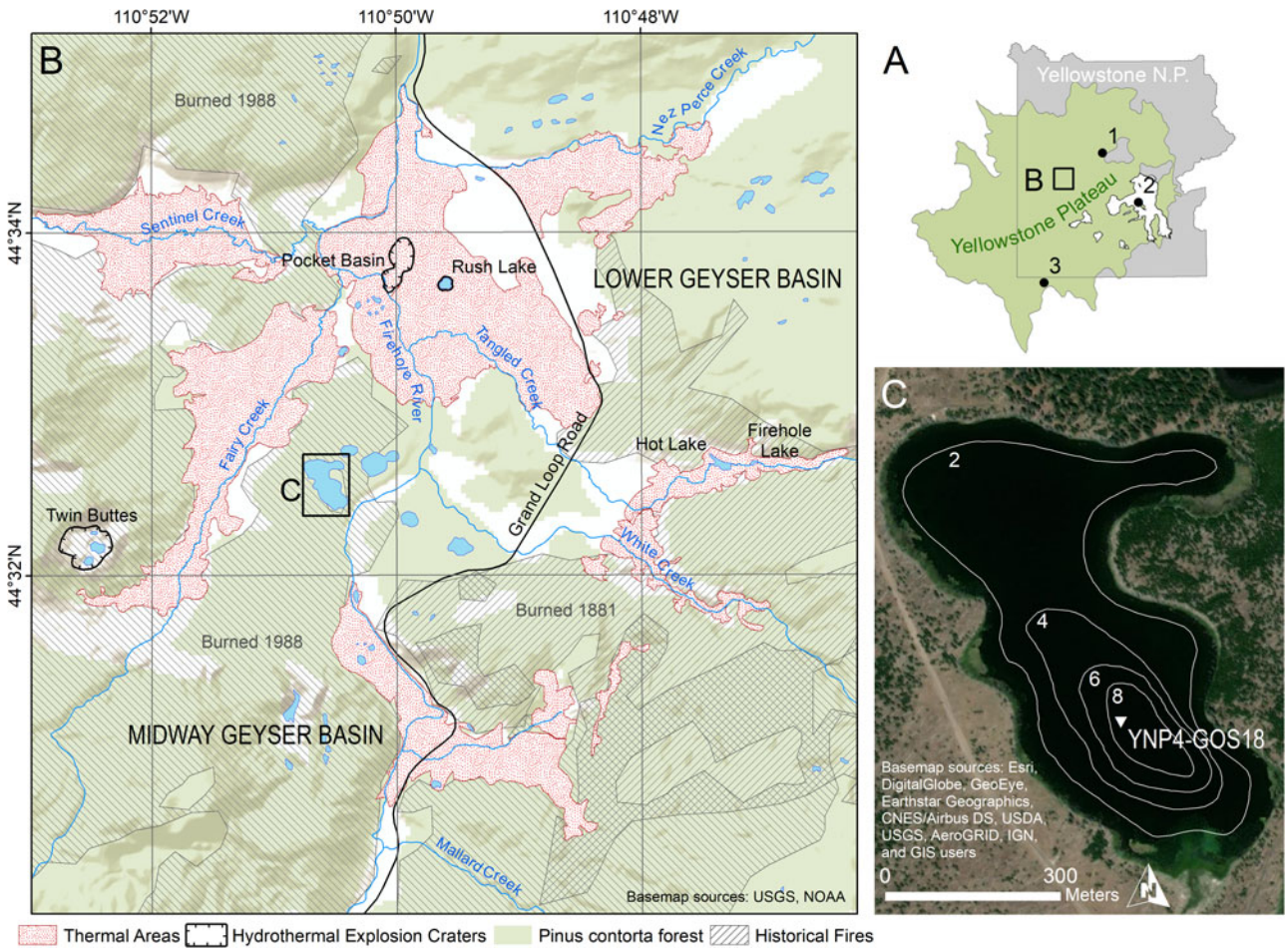

Figure 1. (A) Location of Lower Geyser Basin, Yellowstone National Park, Wyoming, USA, with location of referenced sites (1) Cygnet Lake, (2) Yellowstone Lake, and (3) Loon Lake relative to Yellowstone National Park and the Yellowstone Plateau (an EPA Level IV Ecoregion; Chapman et al., 2004). (B) Goose Lake location within Lower Geyser Basin, and Midway Geyser Basin, with active thermal areas indicated by red stippling (Vaughan et al., 2014), large hydrothermal explosion craters indicated by black ticked outlines (Morgan et al., 2009), pre-AD 1988 extent of *Pinus contorta*-dominated forest in green (Despain, 1990), and extent of historical fires indicated by black hashed lines (Spatial Analysis Center, Yellowstone National Park, 2020). Evidence of hydrothermal activity is pervasive in the Goose Lake vicinity although the lake is not adjacent to any active thermal features. (C) Location of YNP4-GOS18 cores taken in the deepest part of Goose Lake. Bathymetry (m depth) modified from Arnold and Sharpe (1967).

surrounded by post-caldera rhyolite flows (Christiansen and Blank, 1974). Within LGB, rhyolite is overlain by thick Quaternary sediment of glacial and hydrothermal provenance (Bargar and Beeson, 1981; Muffler et al., 1982). The area was covered by the Greater Yellowstone Glacial System during the Pinedale glaciation (locally 22–13 ka, Licciardi and Pierce, 2018). Although the timing of ice retreat in the vicinity of LGB is poorly constrained by absolute ages, the basin was probably ice-free after ~14 ka based on correlation with recessional moraines in northern Yellowstone (Licciardi and Pierce, 2008) and the basal ages of nearby lake sediment cores (Whitlock, 1993). The basin's thermal features have chiefly neutral and alkaline chemistry, with fewer acidic features (http://rcn.montana.edu/Features/Search.aspx, accessed July 2020). Hydrothermal activity has occurred in LGB since at least late Pinedale time, as evidenced by thick hydrothermal deposits interbedded with glacial outwash in drilled cores (Bargar and Beeson, 1981), hydrothermal explosion deposits containing proglacial lake sediments (Muffler et al., 1971), and silica-cemented kame deposits at several localities (Muffler et al., 1982). Several large (>100 m diameter) hydrothermal explosion craters are known from LGB as well, including Twin Buttes, Pocket Basin, and Rush Lake (Muffler et al., 1971; Morgan et al., 2009). Evidence of present and past hydrothermal activity is pervasive throughout the Goose Lake area, including vast flats of silica sinter and diatom ooze (Muffler et al., 1982), but the lake itself is ~280 m from the nearest active thermal features along Fairy Creek to the west (Fig. 1B).

LGB lies within the Yellowstone Plateau, a U.S. Environmental Protection Agency (EPA) Level IV Ecoregion (Chapman et al., 2004) that occupies the central and southwestern portions of Yellowstone National Park as well as adjacent public and private lands to the west and south, and is characterized by rhyolitic substrates and homogeneous forests of *Pinus contorta* (Fig. 1A). Rhyolitic lava flows, such as those surrounding LGB, weather to nutrient-poor, well-drained soils that support *P. contorta* to the near-exclusion of other conifers (Despain, 1990). Within LGB, thermal activity partitions vegetation into zones based on soil temperature and, to a lesser extent, acidity (Miller, 1968; Sheppard, 1971; Rodman et al., 1996). Dense *P. contorta* forests grow where hydrothermal activity is not present and soils are

https://doi.org/10.1017/qua.2021.42 Published online by Cambridge University Press

cool (< 8°C, Rodman et al., 1996; < 12°C, Miller, 1968) as well as patches of *Artemisia tridentata* and *A. tripartita* steppe (Anderson, H.M., personal communication, 2021). Other cool sites underlain by glacial substrate support mixed meadow with mixed grasses and herbs (e.g., *Trifolium repens*, *Rumex acetosella*, *Fragaria* spp., *Prunella vulgaris*, *Chamerion* spp., various Asteraceae; Sheppard, 1971). Unique grassland communities grow in active thermal flats where soil temperatures reach 30–50°C and are dominated by grasses such as *Puccinellia nuttalliana*, *Dichanthelium lanuginosum*, and *Danthonia spicata* that remain diminutive but may grow year-round due to heated surface conditions (Sheppard, 1971; Stout and Al-Niemi, 2002). At the highest soil temperatures (>50°C), grasses are absent and the vegetation mostly consists of mosses (Sheppard, 1971). LGB was extensively burned in AD 1988 and AD 1881, including around the margins of Goose Lake (Spatial Analysis Center, Yellowstone National Park, 2020).

Goose Lake (13.8 ha) has a small inlet stream to the southwest (stream flow < 0.3 m^3/s; |Arnold and Sharpe, 1967) and no surface outlet. Lake bathymetry reveals a broad, shallow bench, comprising up to 80% of the lake bottom, and a maximum depth of 9.5 m (Fig. 1C; Arnold and Sharpe, 1967). The lake's origins are unclear. It may have formed from past hydrothermal processes or in a late Pinedale kettle hole, given that it is surrounded by sandy gravel deposits (Waldrop and Pierce, 1975) interpreted as glacial outwash and kames (Muffler et al., 1982). Other small lakes within a 2 km radius of Goose Lake also appear to be buttressed by kame deposits (Muffler et al., 1982). A recent rise in lake level is evidenced by the presence of dead, submerged pine trees along the shore. *Typha latifolia*, *Scirpus*, and *Carex* grow around the margin of Goose Lake, and *Nuphar luteum*, *Potomogeton* spp., *Myriophyllum* spp., and *Persicaria amphibia* are present as submerged aquatics. In an earlier study by Arnold and Sharpe (1967), water temperatures were measured and ranged from 20.8°C at the surface to 11.6°C at the base of the hypolimnion in July, and pH was 8.1. Previous paleoecological investigations of Goose Lake include an examination of recent diatom assemblages as they relate to fish stocking (Shaw Chraïbi, 2016) and an analysis of charcoal abundance in the surface sediments following the 1988 fires (Whitlock and Millspaugh, 1996).

METHODS

Field sampling

A series of sediment cores (YNP4-GOS18) was collected from an anchored platform in the deepest part of Goose Lake (44.54135° N, 110.84237°W, 8.86 m water depth; Fig. 1C) in June 2018, using a modified Livingstone sampler (Wright et al., 1984). Cores 1A (564 cm long), 1B (100 cm long), and 1D (793 cm long) were extruded, described, and wrapped before being transported from the field. The uppermost sediments were recovered using a gravity sampler in order to retrieve the sediment-water interface, and this short core (20 cm long) was extruded in the field at 1 cm resolution and placed in Whirl-Pak® bags before transport to the lab.

Laboratory analyses

Chronology

Age control was provided by accelerator mass spectrometry (AMS) radiocarbon dating of 22 charcoal samples. Prior to submission, samples were washed with distilled water, cleaned of extraneous material with a dissecting needle under a stereomicroscope, and pretreated with acid-base-acid washes. Samples were not large enough to provide a split for $\delta^{13}C$ analysis. Additional age control also was provided by the age of the sediment-water interface and from tephrochronology.

Lithology and geochemistry

The gravity core and cores 1A, 1B, and 1D were correlated based on depth and lithostratigraphy, particularly using a distinctive, dark, ash-rich siliciclastic layer (Fig. 2). The composite core was 808.5 cm long, and subsequent descriptions use the depths of the composite core. Cores were longitudinally split, imaged, and measured every 0.5 cm for physical parameters (magnetic susceptibility, color, reflectance, density, profile) at the National Lacustrine Core Facility (LacCore, University of Minnesota-Twin Cities), and kept refrigerated except when being sampled or analyzed. Sediments were classified by composition and texture according to the scheme of Schnurrenberger et al. (2003). Measurements were made every 0.5 cm for bulk geochemistry and X-radiographs produced from scanned X-ray fluorescence (XRF) at the Large Lakes Observatory (LLO, University of Minnesota-Duluth). A section of the core with unusually high levels of antimony (Fig. 3) also was analyzed for grain texture using a scanning electron microscope (SEM), elemental composition using SEM-energy-dispersive X-ray spectroscopy (SEM-EDS), and mineralogy using X-ray diffraction (XRD) to help ascertain hydrothermal provenance at the Image and Chemical Analysis Laboratory (ICAL, Montana State University). In addition, $\delta^{13}C$ determinations were done on bulk sediments at the U.S. Geological Survey Stable Isotope Laboratory (Reston, VA) to help ascertain sedimentary carbon provenance.

Pollen analysis

Samples of 0.5 cm^3 were prepared for pollen analysis at intervals of 3 cm to 16.5 cm depth in the core, with the highest sampling resolution in close proximity to ash deposits to explore potential effects of ash falls on vegetation history. Preparation followed standard procedures as outlined in Bennett and Willis (2001). A known concentration of *Lycopodium* spores was added as a spike to calculate pollen concentration (grains/cm^3) and influx (grains/cm^2/yr). Residues were preserved and mounted in silicone oil. At least 300 terrestrial pollen grains and spores were identified at a minimum of 400× magnification and resolved to the lowest possible taxonomic level based on relevant atlases (Hedberg, 1946; Moore et al., 1991; Kapp et al., 2000) and a modern reference collection at Montana State University. Coccal algae palynomorphs were enumerated from synchronous transects of pollen slides.

Pinus grains with visible, intact distal membranes were identified to subgenus. *Pinus* subgen. *Pinus* (diploxylon type, psilate distal membrane) was attributed to *P. contorta*-type, on the grounds that *P. ponderosa* does not presently grow on the Yellowstone Plateau (Arno, 1979). *Pinus* subgen. *Strobus* (haploxylon type, verrucate distal membrane) was attributed to *P. albicaulis*-type, which may include *P. flexilis* that occurs at lower elevations in northern Yellowstone National Park. Cupressaceae grains are assigned to *Juniperus*-type based on the fact that only *J. communis*, *J. horizontalis*, and *J. scopulorum* are present in the region. Percentages of terrestrial pollen were calculated with total terrestrial pollen as a denominator, and aquatic pollen and spores were analyzed as a percent of total pollen

https://doi.org/10.1017/qua.2021.42 Published online by Cambridge University Press

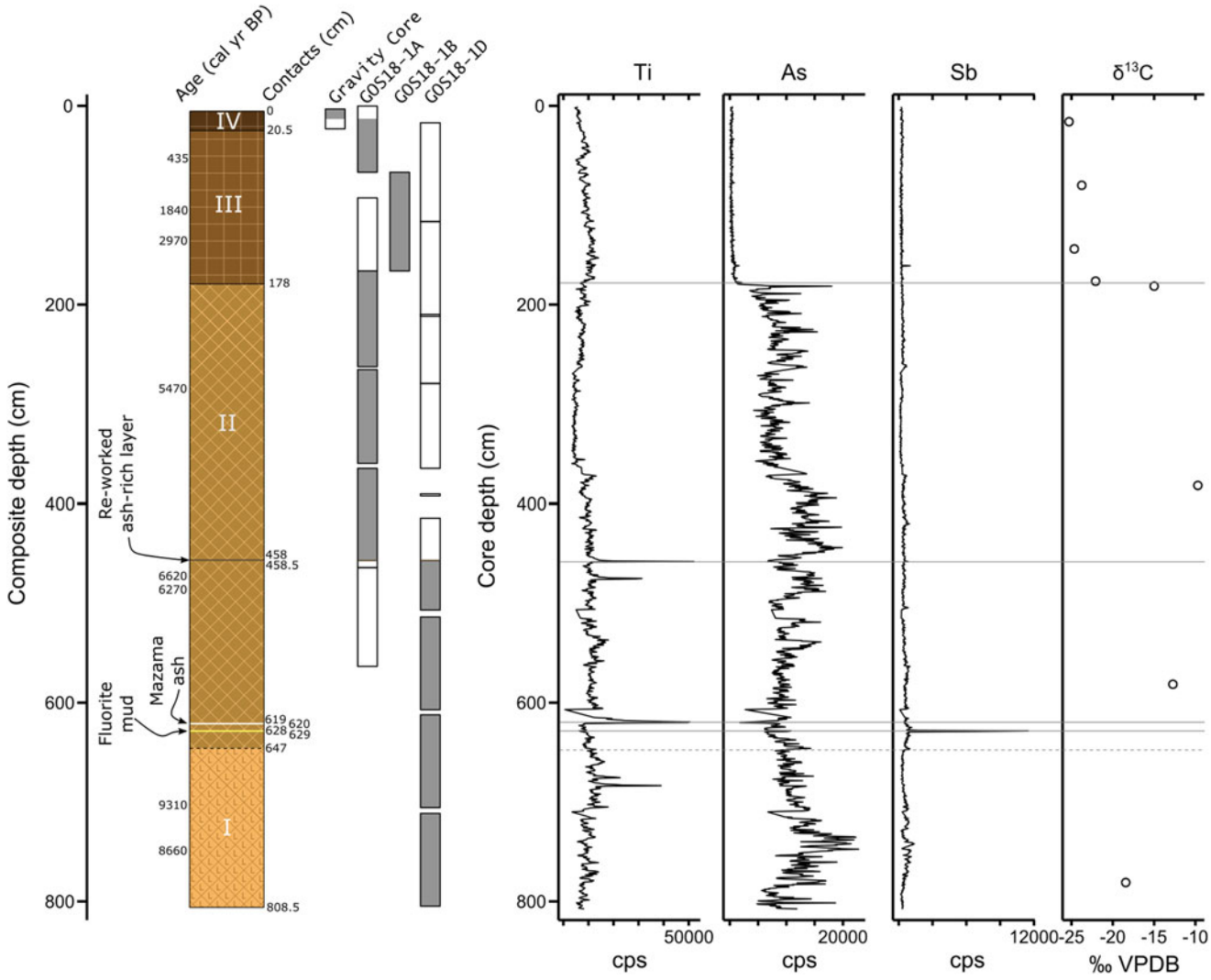

Figure 2. Lithology and geochemistry of the composite Goose Lake core YNP4-GOS18. The core was divided into four stratigraphic units: (I) Indistinctly laminated diatomaceous ooze with clay; (II) Laminated diatomaceous ooze with sapropel and minor, fragmental plant remains, punctuated by antimony-rich fluorite mud (629–628 cm depth), the Mazama ash (620–619 cm depth), and a reworked ash-rich siliciclastic deposit (458.5–458 cm depth); (III) Thinly bedded diatom ooze with sapropel; (IV) Massive diatomaceous sapropel with high water content. The diagram of the composite core is based on core depth, except the correlation between GOS18-1A and GOS18-1D, which was made using the reworked Yellowstone ash. Shaded core drives (gray) were used in developing the composite record. Abundant arsenic is associated with geothermal water influx; and antimony-rich fluorite mud (619–618 cm depth) is definitively of hydrothermal provenance. Higher $\delta^{13}C_{sediment}$ (‰ VPDB) likely indicates an admixture with hydrothermally degassed carbon.

and spores. Coccal algae were identified to the genus level (Jankovská and Komárek, 2000) and analyzed as influx ((number of individual specimens [= NISP])/cm^2/yr), given their great abundance relative to other palynomorphs. Attribution of pollen assemblages to present-day vegetation types was aided by comparison to modern pollen assemblages from the Yellowstone region (Baker, 1976; Whitlock, 1993; Iglesias et al., 2018).

Charcoal analysis

Samples of ~2 cm^3 were collected for charcoal analysis at 0.5 cm intervals for the entire composite core to reconstruct fire history. Charcoal particles >125 µm in diameter were extracted and counted according to standard methodology to analyze long-term trends in charcoal as well as local fire episodes (Whitlock and Millspaugh, 1996; Whitlock and Larsen, 2001). Charcoal accumulation rates (CHAR; measured as particles/cm^2/yr) were calculated with CharAnalysis software for MatLab (Higuera et al., 2009) and were interpreted as an indicator of fire activity or overall time-averaged biomass burned.

The CHAR record was decomposed into background charcoal accumulation rates (BCHAR) representing the long-term trend, and peaks, which are positive deviations above the long-term trend (Higuera et al., 2009, 2011). BCHAR was calculated using a 500-yr locally weighted scatterplot smoothing (lowess) smoother to minimize the sum of the median signal-to-noise index and the goodness-of-fit value, robust to outliers. Variations in BCHAR describe changes in regional biomass burning within tens of kilometers (Higuera et al., 2010), secondarily transported charcoal, and sediment mixing (Whitlock and Larsen, 2001). Charcoal peaks represent fire episodes, individual fires, or a series of fires in close succession within the duration of the charcoal peak. Peaks were considered significant fire episodes if they registered above the 99th percentile of the local noise distribution of CHAR as defined by a Gaussian mixture

https://doi.org/10.1017/qua.2021.42 Published online by Cambridge University Press

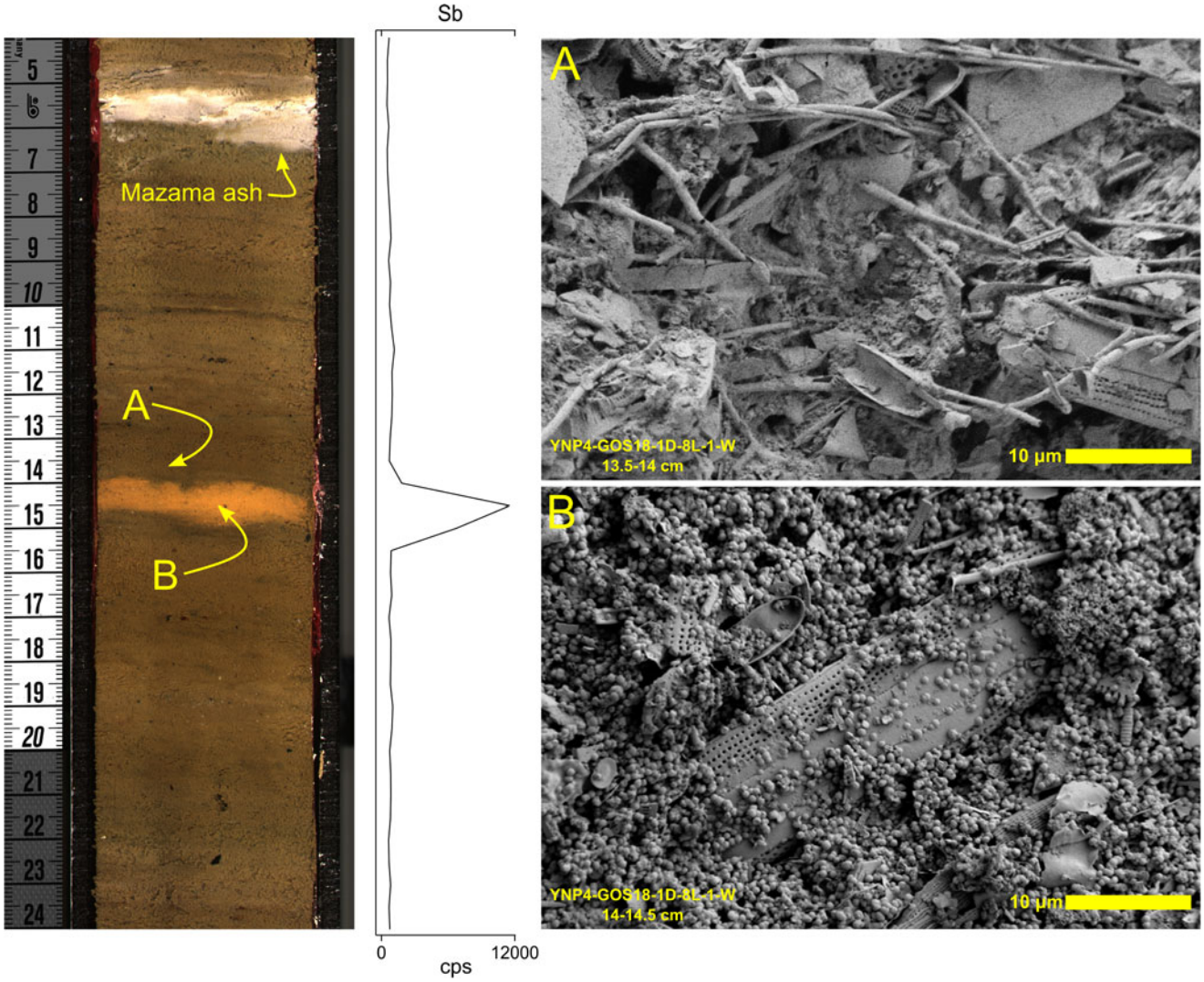

Figure 3. Image of YNP4-GOS18 core section and antimony abundance from scanning XRF analysis including fluorite mud occurring at 628–629 cm depth in the composite core. (A) SEM image of sediment immediately above contact with fluorite mud; note abundant diatom frustules, sponge spicules, and fine-grained clays and organics; (B) SEM image of fluorite mud with 81 wt. % fluorite. Note large diatoms in a matrix of fluorite spherules.

model. Peaks were noted but considered insignificant if they registered between the 95th percentile and 99th percentile. A study of charcoal data from small lakes in the *Pinus contorta* forest of central Yellowstone National Park concluded that charcoal peaks register fire episodes occurring within a 1.2–3.0 km radius around the lake (Higuera et al., 2010)—a highly localized record of fire occurrence. The magnitude of a peak (particles/cm^2) is generally attributed to the fire episode size (area burned) or severity. Peak detection was improved by comparison with the dates of known fires in AD 1988 and AD 1881.

Diatom analysis

Diatom samples of ~0.5 cm^3 volume were collected from the core, ensuring a sample at least every 500 cal yr of the record. Sample preparation consisted of a wash with 30% wt/vol hydrogen peroxide to remove organic matter (Battarbee et al., 2001), and mounting the residue with Naphrax optical adhesive. Diatom valves were identified to species using taxonomic resources relevant to the Northern Rocky Mountains (Bahls, 2005; Spaulding et al., 2020) and general references (Patrick and Reimer, 1975). A total of 300 diatom valves were enumerated per slide and analyzed as a percent of the diatom sum. Lake conditions inferred from the diatom community were based on species-level autecology.

RESULTS

Chronology

The Goose Lake age-depth model was based on 15 of 22 AMS radiocarbon ages, the age of the sediment-water interface, and the known age of Mazama ash (Egan et al., 2015) (Table 1, Fig. 4). Radiocarbon ages were calibrated with the IntCal13 calibration curve and verified against IntCal20 (Reimer et al., 2013, 2020). A preliminary chronology suggested that some of the radiocarbon-dated samples were anomalously old. On the assumption that sediment accumulated over time without reversals and the age of Mazama ash was most reliable, we took a Bayesian approach to enforce a montonic model. We constrained

https://doi.org/10.1017/qua.2021.42 Published online by Cambridge University Press

Table 1. Goose Lake core age determinations. All numbered samples were measured at NOSAMS Laboratory at the Woods Hole Oceanographic Institution. Calibrated age ranges were calculated with CALIB ver. 7.1 (Stuiver et al., 2019) and age ranges with probabilities <0.01 are excluded.

Accession No.	Core/Depth (cm)	Material Dated	Age ^{14}C	2σ cal Age Range (Probability)
	0.0	Core top		−68
OS-144345	41.25	charcoal	435 ± 55	316–399 (0.227), 422–545 (0.773)
OS-144559	107.75	charcoal	1840 ± 65	1609–1902 (0.989), 1910–1923 (0.011)
OS-144382	149.75	charcoal	2970 ± 20	3071–3185 (0.931), 3190–3209 (0.069)
OS-146794*	208.75	charcoal	8050 ± 340	8171–9709 (0.998)
OS-146796	263.0	charcoal	5390 ± 140	5893–6478 (1.000)
OS-144560	294.25	charcoal	5470 ± 150	5919–6565 (0.996)
OS-146789*	341.5	charcoal	7070 ± 190	7575–8218 (0.974), 8240–8305 (0.026)
OS-144561*	393.75	charcoal	3870 ± 120	3923–4614 (0.994)
OS-146790	472.25	charcoal	6620 ± 190	7160–7867 (0.993)
OS-146813	482.25	charcoal	6270 ± 35	7029–7043 (0.010), 7087–7111 (0.015), 7155–7272 (0.971)
OS-146791*	518.75	charcoal	8390 ± 330	8560–10,197 (1.000)
OS-146792*	536.25	charcoal	8500 ± 230	8989–10,192 (1.000)
	620.0	Mazama ash		7584–7682[1]
OS-146793*	647.5	charcoal	9400 ± 290	9763–11,407 (0.993)
OS-146795*	698.25	charcoal	9310 ± 330	9552–11,362 (0.998)
OS-146814	744.25	charcoal	8660 ± 50	9531–9744 (1.000)

[1]Calibrated age range from Egan et al. (2015)
*Age outside of 95% range of final age-depth model; not used in final age model

sediment accumulation rates to positive values by setting an a priori distribution for sediment deposition time with a mean of 10 yr/cm^{-1} and a shape of 1.5 (Blaauw and Christen, 2011). Reversals in radiocarbon ages were addressed by using Student's *t*-distributions with heavier tails for our calibrated ages ($t_a = 3$, $t_b = 4$) than for the ages of the tephra ($t_a = 33$, $t_b = 44$) (Christen and Pérez, 2009). This approach allowed us to inform the model that the ages of the known tephra were more precise than other ages and to increase their influence on the chronology accordingly (Blaauw et al., 2018). Finally, we used splines to model depth from the explicitly combined probability distribution of all ages (Blaauw and Christen, 2011).

Age reversals were present in the core below 178 cm depth, and seven radiocarbon dates were rejected by the Bacon model (Fig. 4). All but sample OS-144561 were interpreted as erroneously old. The cause of these erroneously old ages is not clear, but old carbon contamination has been documented within the Yellowstone caldera in lake sediments (Schiller et al., 2021) and in organic material entombed in silica sinter (Churchill et al., 2020). It is likely that Goose Lake samples contained old carbon sourced from either reworked sediment, volcanic CO_2 incorporated into plants during photosynthesis (Evans et al., 2010), or volcanic CO_2 in the water column and surficial sediments (Schiller et al., 2021).

To address the uncertainty of point estimates of age from the age-depth model, median calibrated ages with standard deviations >100 yr were rounded to the nearest 100 cal yr. The extrapolated age-depth model suggests a basal core age of 10,300 cal yr BP. A Holocene age is consistent with the fact that the basal pollen spectra were dominated by *Pinus contorta*-type, which was first abundant in Yellowstone Plateau pollen records after ca. 11,500 cal yr BP (Whitlock, 1993; Iglesias et al., 2018). Two changes in sediment accumulation rate were noted. Sediment accumulation rates sharply increased between 6000 cal yr BP and 4000 cal yr BP, potentially driven by a lithological change, such as the contact between Unit II and III at 178 cm depth. The change in sediment accumulation rate following Mazama ash deposition at 620 cm depth is probably an artifact of the high confidence placed on the age of the Mazama ash and the high statistical influence of the basal radiocarbon date, making age determinations below the Mazama ash potentially dubious and are aptly treated with caution hereafter.

Lithology and geochemistry

Unit I (808.5–647 cm depth; 10,300–8200 cal yr BP) consisted of light olive-brown (2.5Y 5/3), indistinctly laminated diatomaceous ooze with clay (Fig. 2). Diatoms and sponge spicules were dominant in smear slides. Diatoms were mostly intact. Peaks in sediment titanium, a non-biologically active element relatively abundant in siliciclastic sediments (Kylander et al., 2011), were associated with lenses of inorganic clay, and arsenic was relatively

https://doi.org/10.1017/qua.2021.42 Published online by Cambridge University Press

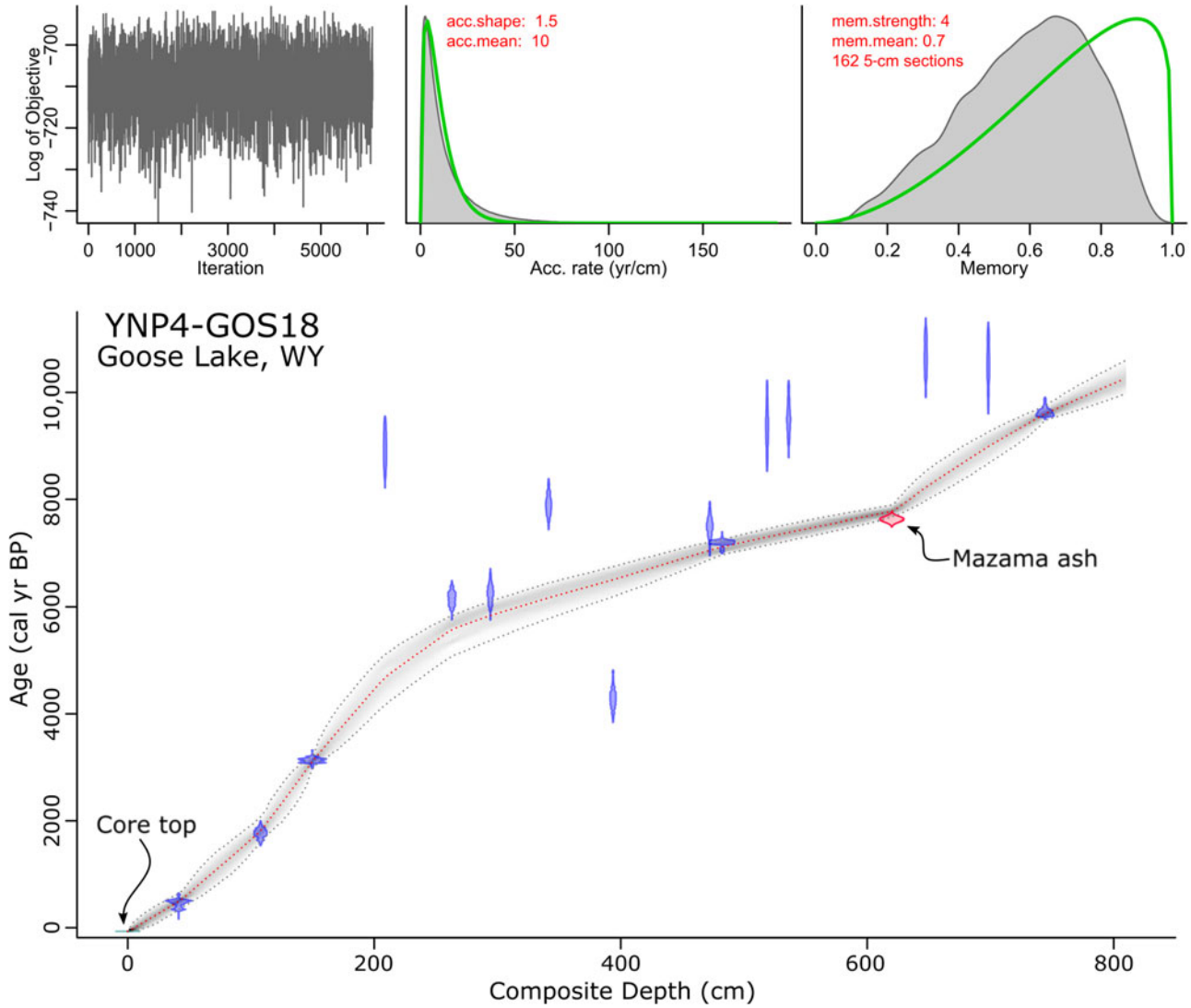

Figure 4. Bacon age-depth model for Goose Lake composite core YNP4-GOS18. Probability distributions are plotted for the core top (light blue horizontal line), calibrated radiocarbon ages (blue distribution curves), and the Mazama ash (red distribution curve). Red dashed line is the median probability age from all run age-depth iterations, representing the best point estimate of age for any given depth, which is used for remaining plots. Gray point cloud represents age model probability and contains a 95% confidence interval (dashed gray lines). Iteration history (left top), prior and posterior densities of the mean accumulation rate (middle top), and prior and posterior of the memory (right top) suggest reasonable adherence of the model to a priori mean accumulation rate and memory assignments.

abundant throughout the interval. $\delta^{13}C_{sediment}$ was measured at −18.43 ‰ VPDB.

Unit II (647–178 cm depth; 8200–3800 cal yr BP) consisted of laminated diatomaceous ooze with sapropel and minor fragmental plant remains (Fig. 2). Diatoms and sponge spicules were dominant in smear slides. Laminations were alternately grayish-brown (2.5Y 5/2), dark reddish-brown (5YR 3/2), and gray (GLEY1 5/N). Titanium peaks were associated with siliciclastic deposits, including ashes and inorganic clay layers. Arsenic was abundant throughout the unit. $\delta^{13}C_{sediment}$ values averaged −12.47 ‰ VPDB. An orange, inorganic clay was noted in the composite core at 628–629 cm depth (7900 cal yr BP; Fig. 3). XRD analysis indicated 81.1 wt % fluorite (hereafter fluorite mud, as an unconsolidated sediment mostly composed of inorganically precipitated fluorite), and SEM-EDS measurements confirmed abundant calcium and fluorine. The remaining weight fraction consisted of silica. SEM photomicrographs revealed diatom frustules and sponge spicules in a matrix of fluorite spherules (~0.5 µm matrix grain size, Fig. 3). The fluorite mud was notably enriched in antimony relative to the other Goose Lake sediments as indicated by XRF measurements (Fig. 3).

Two distinct siliciclastic deposits were noted in Unit II at 620–619 and 458.5–458 cm depth (Fig. 2). The lower deposit was white and composed of glass (~100%, much of which is pumiceous) with trace amounts of plagioclase, an unknown green (?)phyllosilicate, and quartz. Geochemistry of glass shards from electron microprobe analysis determined this deposit to be the Mazama ash (Iverson, N.A., personal communication, 2019). The upper deposit, which we used for correlation between cores 1A and 1D, was dark colored and a compositional mixture of lacustrine sediment, reworked minerogenic sediment, and ash. Felsic mineral abundance (siliciclastic fraction: quartz, ~60%; ash, ~40%; <1% each plagioclase, potassium feldspar, and clinopyroxene) and lacustrine components suggest a local rhyolitic source that

https://doi.org/10.1017/qua.2021.42 Published online by Cambridge University Press

was reworked and redeposited into Goose Lake, perhaps from surface run-off or a mass-wasting event.

Unit III (178–20.5 cm depth; 3800–200 cal yr BP) consisted of dark olive-brown (2.5Y 3/3), thinly bedded diatom ooze with sapropel (Fig. 2), containing abundant diatom frustules and chrysophytes. Biogenic sediment components, notably diatom frustules, were highly fragmented in this unit, many <2–5 µm in diameter. Highly fragmented diatom frustules suggest grazing by amphipods (e.g., *Gammarus*) (Quigley and Vanderploeg, 1991), which are abundant in modern Goose Lake (Arnold and Sharpe, 1967). $\delta^{13}C_{sediment}$ values were considerably lower than underlying units, −23.05 ‰ VPDB on average.

Unit IV (20.5–0 cm depth; 200 – −68 cal yr BP) consisted of very dark grayish-brown (2.5Y 3/2), massive diatomaceous sapropel with high water content (Fig. 2). Diatom frustules were relatively intact, and the $\delta^{13}C_{sediment}$ value was similar to the previous interval, −25.30 ‰ VPDB.

Biological proxies

The pollen data from Goose Lake were divided into three zones based on visual inspection and using CONISS, a stratigraphically constrained cluster analysis (Grimm, 1987) (Fig. 5). These zones are used as a framework to describe all biological data.

Zone GOS1 (808.5–618 cm depth, 10,300–7800 cal yr BP)

Pinus dominated the pollen spectra (77%, excluding a sample immediately above the Mazama ash; Fig. 5), mostly assigned to *P. contorta*-type (81% of *Pinus* grains identifiable to subgeneric level). *Artemisia* (<13%), Amaranthaceae (<3%), and Poaceae (<2%) pollen were present in smaller proportions. A pollen sample immediately above the Mazama ash consisted of more *Artemisia* (51%) than *Pinus* (34%) pollen, and was the only sample from the record where the sum of nonarboreal pollen exceeded arboreal pollen types, suggesting a brief (<8 yr, based on average sediment accumulation rate for 1 cm) vegetation change following ashfall. CHAR (mean 1.4 particles/cm^2/yr) was generally low (Fig. 5), although the uppermost CHAR values were probably artificially deflated by the rapid increase in sediment accumulation time noted above (Fig. 4). Mean fire frequency reached its highest values of the record (14 episodes/1000 yr).

The diatom record consisted of *Cyclotella meneghiniana* (28%) and *Diatoma moniliformis* (21%), with lesser amounts of *Navicula wildii* (12%), *Amphora copulata* (9%), *Gomphonema gracile* (7%), and *Achnanthidium minutissimum* (7%) (Fig. 6). The lower portion of Zone GOS1 was dominated solely by *C. meneghiniana* (Fig. 6), but by mid-zone, *C. meneghiniana* abundance decreased and *D. moniliformis* and *N. wildii* co-dominated. *Botryococcus* (89,981 NISP/cm^2/yr) dominated the coccal algae assemblage with few *Pediastrum* (56 NISP/cm^2/yr) (Fig. 6).

Zone GOS2 (618–178 cm depth, 7750–3800 cal yr BP)

Pinus percentages increased in Zone GOS2, with abundance reaching 84% at the top of the zone (Fig. 5). *P. contorta*-type accounted for 93% of the identifiable *Pinus*. Increased *Pinus* percentages came at the expense of upland herb taxa, with lower abundances of *Artemisia* (<9%), Amaranthaceae (<2%), and Poaceae (<2%) compared to Zone GOS1. A horizon rich in degraded, indeterminate herbaceous pollen grains (457.5 cm depth, 6950 cal yr BP) was associated with the siliciclastic deposit at 458 cm depth, likely reflecting significant pollen reworking during the same depositional event. CHAR (mean 3.5 particles/cm^2/yr) substantially increased from Zone GOS1 (Fig. 5), and mean fire frequency was lower than before (13 episodes/1000 yr).

The diatom record shows a loss of *Cyclotella meneghiniana*, and persistence of *Diatoma moniliformis* (17%), *Gomphonema gracile* (17%), *Amphora copulata* (16%), *Navicula wildii* (13%), and *Achnanthidium minutissimum* (12%) (Fig. 6). Additionally, an upper portion of Zone GOS2 (225–178 cm depth, 4970–3960 cal yr BP) contained a peak in *Encyonema yellowstonianum* (9%) and a synchronous increase in *Pseudostaurosiropsis* sp. (16%). The coccal algae assemblage consisted of *Botryococcus* (20,211 NISP/cm^2/yr) and *Pediastrum* (3167 NISP/cm^2/yr) (Fig. 6).

Zone GOS3 (178–0 cm depth, 3800– -68 cal yr BP)

Zone GOS3 was characterized by less *Pinus* than before (72%), predominantly *P. contorta*-type (95% of *Pinus* identifiable to subgeneric level) (Fig. 5). Major upland herb taxa concurrently increased in abundance, including *Artemisia* (<16%), Amaranthaceae (<3%), and Poaceae (<4%), with *Ambrosia*-type (<1%) and Asteraceae subfam. Asteroideae (<1%) present in low amounts. Pollen of riparian shrubs *Alnus*, *Betula*, and *Salix* were also present in trace amounts (<1%). *Arceuthobium* (<1%) was consistently detected for the first time in Zone GOS3. CHAR values (mean 9.6 particles/cm^2/yr) were the lowest in the record (Fig. 5). Mean fire frequency also declined from previous zones to 10 episodes/1000 yr. The median calibrated ages from the two uppermost CHAR peaks (AD 1988–1948, AD 1903) correlate well with fires in AD 1988 and AD 1881 within LGB.

The Zone GOS3 diatom assemblage was dramatically different than previous zones and dominated by *Pinnularia microstauron* (14%) and *Stauroneis americana* (31%) (Fig. 6). Diatom abundance was lower in Zone GOS3 compared to previous zones, whereas chrysophyte cysts were more abundant. The coccal algae assemblage was dominated by *Pediastrum* (15,294 NISP/cm^2/yr) with a lesser amount of *Botryococcus* (1880 NISP/cm^2/yr) (Fig. 6).

DISCUSSION

In reconstructing the Holocene history of LGB, we utilize geochemical and lithological data from Goose Lake to describe changes in hydrothermal activity within and near the lake. The pollen and charcoal records are used to reconstruct the basin's vegetation and fire history, which is then compared with other sites on the Yellowstone Plateau to separate the influence of local geologic versus regional climatic drivers on ecosystem dynamics. The diatom record describes shifts in the limnobiotic conditions of Goose Lake.

Past hydrothermal activity at Goose Lake

Thermal waters flowed into Goose Lake from ca.10,300 cal yr BP to 3800 cal yr BP, based on geochemical and lithologic data. Arsenic is abundant in lithological units I and II that date to this period, and is similarly abundant in hydrothermally influenced sediments elsewhere on the Yellowstone Plateau (Shanks et al., 2007; Morgan et al., 2009), as well as in present-day thermal waters in LGB (Planer-Friedrich et al., 2006). In addition, antimony-rich fluorite mud, deposited briefly ca. 7900 cal yr BP (619–618 cm depth), is definitively of hydrothermal provenance, inasmuch as fluorite is a secondary hydrothermal mineral in the rhyolite flows that underlie Goose Lake (Bargar and Beeson, 1981), and antimony is abundant in geothermal waters from

https://doi.org/10.1017/qua.2021.42 Published online by Cambridge University Press

https://doi.org/10.1017/qua.2021.42 Published online by Cambridge University Press

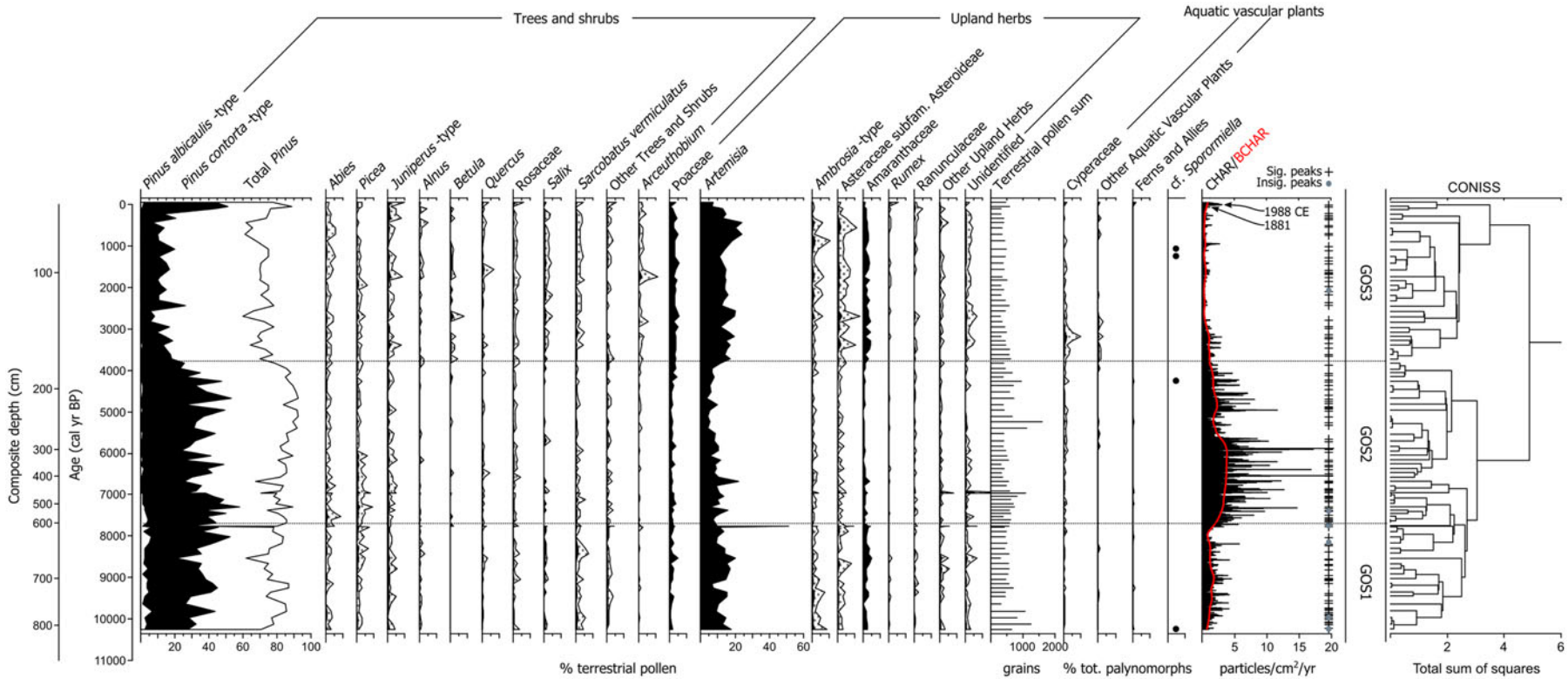

Figure 5. Percentage diagrams of major pollen types and spores (>1%), total sum of terrestrial pollen, and charcoal data (CHAR and BCHAR) with significant and insignificant peaks from Goose Lake composite core YNP4-GOS18. Where present, curve exaggeration is 5×. Zone delineation is supported by CONISS dendrogram constructed with percentage data from terrestrial pollen.

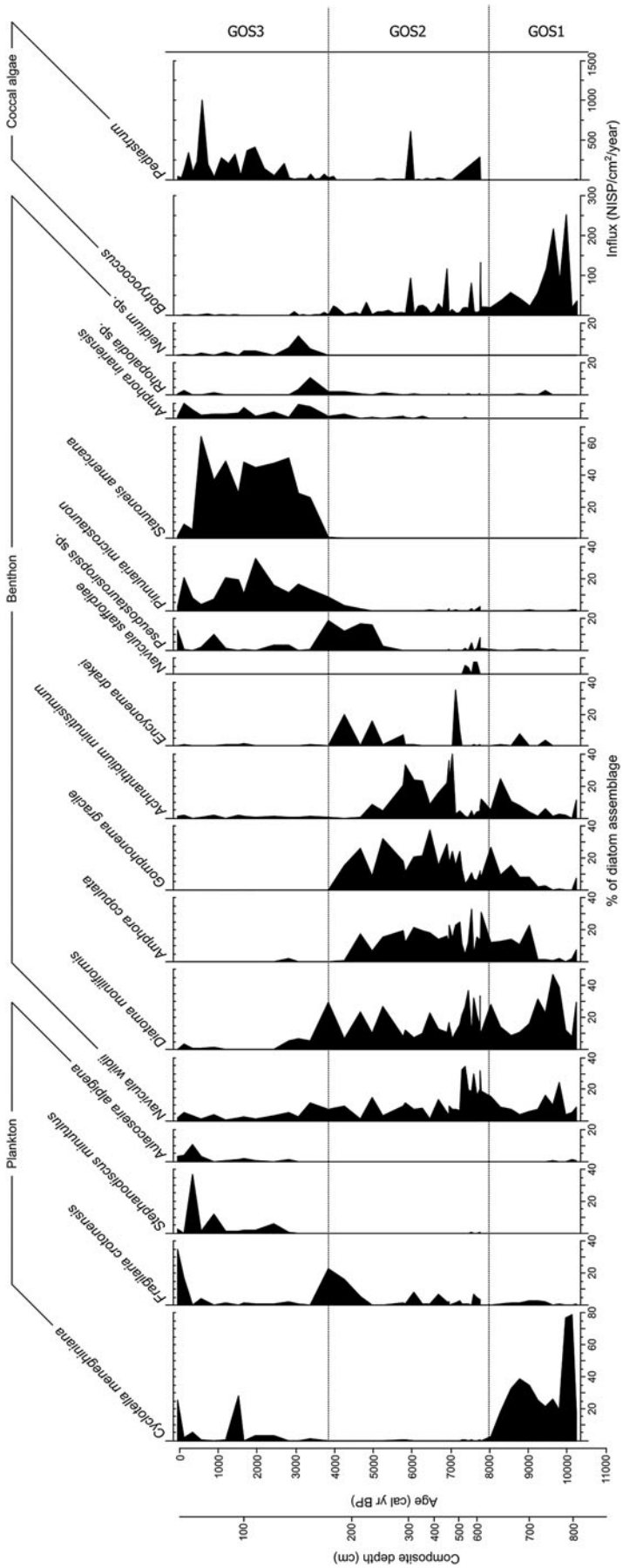

Figure 6. Diagram of major diatom species percentages and influx (NISP/cm^2/yr) of coccal algae from Goose Lake composite core YNP4-GOS18.

https://doi.org/10.1017/qua.2021.42 Published online by Cambridge University Press

Table 2. Paleoecological sites and reference sources from within *Pinus contorta* forest site from Yellowstone National Park and the Yellowstone Plateau (an EPA Level IV Ecoregion; Chapman et al., 2004) used for comparison purposes with Goose Lake data.

Site	Location	Elevation (masl)	Modern vegetation	Source
Loon Lake	44.11°N 110.94°W	1968	*Pinus contorta* forest with *Pseudotsuga menziesii*	Whitlock et al., 1995*
Cygnet Lake	44.39N 110.36W	2530	*Pinus contorta* forest	Whitlock, 1993*; Millspaugh et al., 2000†
Yellowstone Lake	44.5°N 110.3°W	2350	Forest-meadow mosaic with abundant *Pinus contorta*	Theriot et al., 2006*

*Source of pollen data
†Source of charcoal data

LGB (Stauffer and Thompson, 1984). Lithologic units I and II also have higher $\delta^{13}C_{sediment}$ values (−18.43 ‰ VPDB; −9.7 ‰ VPDB) than overlying units, pointing to an admixture of hydrothermally degassed carbon (∼−3 ‰ VPDB; Bergfeld et al., 2014), which is higher than terrestrial vegetation (Smith and Epstein, 1971), and terrestrial or aquatic organic carbon. In addition, the more distinct laminations (Fig. 2) of sediments in Unit I and, especially, Unit II suggest frequently shifting limnological conditions as might be produced by intermittent inputs of thermal water relative to meteoric and groundwater sources. Sediments remain lacustrine in character with abundant diatom frustules and sponge spicules in Units I and II. Thus, Goose Lake during this interval was adjacent to or supported sublacustrine thermal features. The presence of a benthic lacustrine community indicates that it was not a large thermal spring, such as present-day Firehole Lake or Hot Lake in LGB (Fig. 1B).

Goose Lake hydrothermal activity ceased abruptly at ca. 3800 cal yr BP. Diminished arsenic abundance, lower $^{13}C_{sediment}$ values (−25.30 ‰ VPDB; −22.08 ‰ VPDB), and darker sediments composed of diatoms and chrysophytes in lithologic Units III and IV suggest quiescent lake sedimentation without hydrothermal influence (Fig. 2). The abruptness of this transition is inferred from the sharp contact between lithologic Units II and III.

Development of the LGB geo-ecosystem with regional context

To determine the relative importance of local hydrothermal activity versus regional climate change in shaping the environmental history of LGB, we compared the Goose Lake data with three other paleoecological records from the Yellowstone Plateau. We assumed that concurrent and similar paleoecological changes across many sites point to a regional forcing, such as climate change. When a vegetation change occurred only at one site, the forcing was likely local, such as changing hydrothermal activity.

The vegetation record at Goose Lake was compared with nearby sites that lack significant surficial hydrothermal activity: Cygnet Lake (Whitlock, 1993; Millspaugh et al., 2000), Loon Lake (Whitlock et al., 1995), and Yellowstone Lake (Theriot et al., 2006) (Fig. 1A, Table 2). Yellowstone Plateau forests are dominated by *Pinus contorta*, but the admixture of *Pseudotsuga menziesii* at Loon Lake and *Abies lasiocarpa* and *Picea engelmannii* at Yellowstone Lake necessitates acknowledgement of other arboreal forest components. Therefore, we used a standardized ratio of arboreal pollen (AP) to non-arboreal pollen (NAP) types (AP:NAP, $^{AP - NAP}/_{AP + NAP}$) to infer past forest cover (openness or extent) at each site. A lowess smoother (x ∼ y) was applied to each AP:NAP data set to emphasize long-term trends.

A charcoal-based fire history at Cygnet Lake provides a reasonable comparison for that at Goose Lake, given that the site is similar in size and also surrounded by *Pinus contorta* forest (Millspaugh et al., 2000). CharAnalysis was conducted for Cygnet Lake charcoal data in the same manner as for Goose Lake, except BCHAR values at Cygnet Lake were calculated with the use of a 700-yr lowess smoother robust to outliers, which minimized the sum of the median signal-to-noise index and the goodness-of-fit value. New age models were created for Cygnet, Loon, and Yellowstone Lakes utilizing IntCal13 (Reimer et al., 2013) and Bacon (Blaauw and Christen, 2011), and sediment accumulation rate priors that closely approximated inferences from the original publications (Whitlock, 1993; Whitlock et al., 1995; Millspaugh et al., 2000; Theriot et al., 2006).

Holocene climate context on the Yellowstone Plateau

The Holocene climate of the Yellowstone Plateau was strongly influenced by slow variations in the seasonal cycle of precession, which led to a summer insolation maximum in the Northern Hemisphere at ca. 11 ka and a steady decline thereafter (Laskar et al., 2004). The Yellowstone Plateau has a summer-dry precipitation regime (Whitlock and Bartlein, 1993), and the summer insolation maximum (summer anomaly up to ∼30 W/m^2 at 44.5°N; Laskar et al., 2004) in this region resulted in warmer and effectively drier conditions than the twentieth century average as a result of the expansion and strengthening of the northeastern Pacific subtropical high-pressure system (Whitlock and Bartlein, 1993; Bartlein et al., 1998). In the middle and late Holocene, summers on the Yellowstone Plateau became cooler and effectively wetter due to declining summer insolation and the attendant weakening of the northeastern Pacific subtropical high, leading to the establishment of present climate conditions (Whitlock and Bartlein, 1993; Bartlein et al., 1998). Paleoclimate reconstructions from the Yellowstone National Park vicinity corroborate a story of warm, dry conditions in the early Holocene that became increasingly cool and wet to the present (Larsen et al., 2020; Chellman et al., 2021).

Early Holocene (GOS1, >10,300–7800 cal yr BP)

Pollen records from Cygnet Lake, Loon Lake, and Yellowstone Lake indicate that surrounding forests were relatively open or less extensive, as evidenced by depressed AP:NAP values at all sites compared with the Holocene average from the area (Fig. 7; Whitlock, 1993; Whitlock et al., 1995; Theriot et al., 2006). The landscape at Goose Lake was similarly open, as indicated by similarly low AP:NAP (Fig. 7). Forests around Goose Lake were dominated by *Pinus contorta* as they are at present, as indicated by a

https://doi.org/10.1017/qua.2021.42 Published online by Cambridge University Press

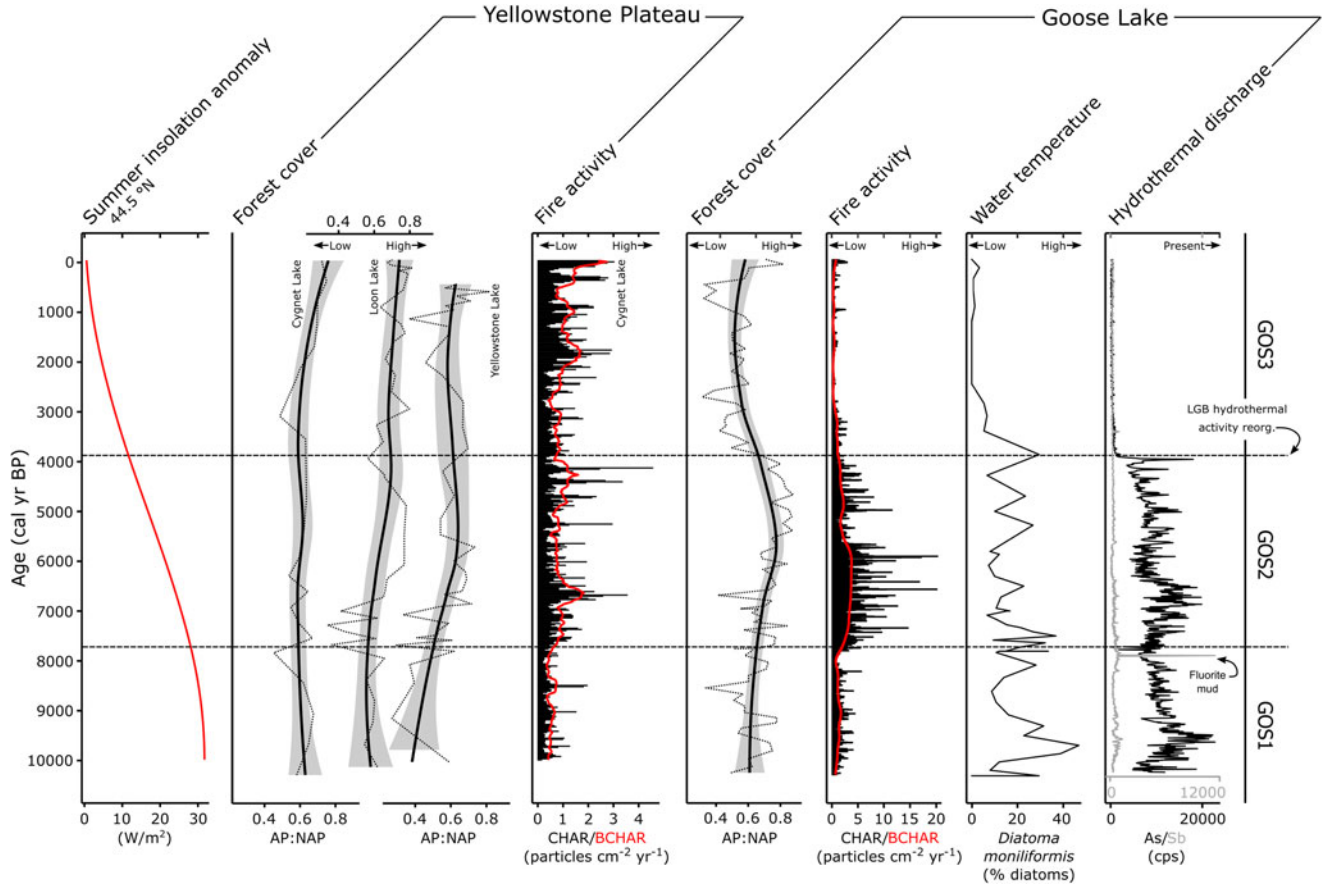

Figure 7. Comparison plot of proxy data from the Goose Lake composite core YNP4-GOS18 with other sites on the Yellowstone Plateau (Cygnet Lake, Loon Lake, Yellowstone Lake). Seasonal insolation anomaly calculated for 44.5°N (Laskar et al., 2004). Forest cover at sites without significant surficial hydrothermal activity (Whitlock, 1993; Whitlock et al., 1995; Theriot et al., 2006) is plotted as standardized AP:NAP ratios ($^{AP - NAP}/_{AP + NAP}$; dotted line) with lowess smoother (solid line with shaded 95% confidence interval); fire activity at Cygnet Lake (Millspaugh et al., 2000; CHAR in black, BCHAR in red). Forest cover and fire activity plots for Goose Lake are juxtaposed with diatom and geochemical indicators of hydrothermal conditions.

dominance of *Pinus* pollen (Fig. 5). The deposition of the Mazama ash at 7630 cal yr BP (Egan et al., 2015) led to a short-term proliferation of *Artemisia*, as evidenced by the spike in *Artemisia* percentages immediately above the ash. This spike is attributed to short-lived mulching effects of volcanic ash on the landscape, and has been noted in records throughout the northern Rocky Mountain region (Schiller et al., 2020). The charcoal record from Cygnet Lake shows that fire activity was generally low in the early Holocene as evidenced by the lowest CHAR of the record (mean CHAR 0.53 particles/cm^2/yr). Fire activity at Goose Lake was similarly low in this period compared with the rest of the record based on BCHAR data, and fire frequency was the highest of the record (Fig. 7). Fires were frequent but relatively small or low in severity.

The diatom data indicate that Goose Lake was shallower than at present, with oligotrophic to mesotrophic conditions in the early Holocene. *Cyclotella meneghiniana*, *Amphora copulata*, and *Achnanthidium minutissimum* are favored by oligotrophic to mesotrophic conditions at present (Parsons et al., 2006; Salm et al., 2009; Saros and Anderson, 2015). *C. meneghiniana* populations are abundant in well-mixed or relatively shallow lakes (Reynolds, 1980), and bloom in response to influxes of nitrogen and phosphorous (Salm et al., 2009). The presence of *Diatoma moniliformis* is consistent with water temperatures greater than 10–15°C (Pniewski and Sylwestrzak, 2018) and/or harsh conditions (e.g., the species is found in nuclear power-plant cooling channels; Potapova and Snoeijs, 1997). Another benthic species, *Navicula wildii*, prefers neutral to moderate alkalinity (Bahls, 2012), and *Achnanthidium minutissimum* is present in a wide variety of pH conditions (Ponader and Potapova, 2007). *Gomphonema gracile* is a cosmopolitan benthic species (Patrick and Reimer, 1975). The assemblage, along with its good preservation (i.e., diatoms are destroyed under strongly alkaline conditions) indicates that the water pH was neutral to slightly alkaline, similar to that of most LGB thermal waters at present (Hurwitz and Lowenstern, 2014). The dominance of *C. meneghiniana* from 10,300 cal yr BP to 9800 cal yr BP suggests an initial period of high nutrient input, and the later abundance of low-nutrient specialist *Amphora copulata* implies decreasing nutrient availability after 9420 cal yr BP.

Botryococcus was abundant in Goose Lake in the early Holocene and *Pediastrum* was nearly absent; an assemblage often interpreted as evidence of extremely cold, oligotrophic, or acidic waters (Jankovská and Komárek, 2000). Those conditions seem unlikely at this time in Goose Lake in light of the diatom assemblage, which suggests neutral to alkaline water chemistry and inferred warm, dry summers (Whitlock and Bartlein, 1993). However, high levels of arsenic in the water column may explain

https://doi.org/10.1017/qua.2021.42 Published online by Cambridge University Press

the *Botryococcus* abundance. Some modern waterways contaminated by anthropogenic (Meeinkuirt et al., 2008) or naturally occurring (Miller, 2020) arsenic have abundant *Botryococcus*, with little to no noted *Pediastrum*. *B. braunii* has even shown some promise as a bioremediator of environmental arsenic (Onalo et al., 2014; Podder and Majumder, 2016). Taken together, the diatom and coccal algae assemblages indicate warm, somewhat alkaline, and arsenic-rich conditions associated with thermal water discharge into Goose Lake.

In summary, early Holocene vegetation at Goose Lake resembled that of the Yellowstone Plateau as a whole, with relatively open *Pinus contorta* forest or expanded non-forested vegetation as a result of warm, dry conditions and frequent small or low-severity fires. Thermal waters discharged directly into Goose Lake, as evidenced by the geochemical and lithological characteristics of the sediments and limnobiotic communities, but hydrothermal activity did not alter the upland vegetation to a large extent.

Middle Holocene (GOS2, 7750–3800 cal yr BP)

Increasing AP:NAP values from Cygnet Lake, Loon Lake, and Yellowstone Lake suggest that forest became more closed or more extensive across the Yellowstone Plateau in the middle Holocene (Whitlock, 1993; Whitlock et al., 1995; Theriot et al., 2006; Fig. 7). At Goose Lake, the forest also became more closed or extensive through this period, with similarly increasing AP:NAP values (Fig. 7) and continued dominance of *Pinus* pollen (Fig. 5). An increase in fire activity at Cygnet Lake, as evidenced by rising BCHAR, was coupled with particularly extreme (large or severe) fire episodes based on high charcoal peak magnitudes (Millspaugh et al., 2000). The same interpretation can be drawn at Goose Lake, where the charcoal data indicate large or severe, but infrequent, fires (Fig. 7).

The middle Holocene diatom assemblage at Goose Lake is similar to that of the early Holocene, except for the conspicuous absence of *Cyclotella meneghiniana*. The dominance of benthic taxa suggests a change in water level, but it is difficult to know if water level rose or fell, given the broad, flat bathymetry of Goose Lake (Fig. 1C). Persistence of species with warm-water preferences (*Diatoma moniliformis*) and wide pH tolerance ranges (*Achnanthidiuim minutissimum*, *Navicula wildii*, and *Pseudostaurosiropsis* sp.) (Ciniglia et al., 2007) indicates that the diatom assemblage continued to be influenced by thermal inputs through this period. Low nutrient availability is indicated by *Achnanthidiuim minutissimum* and *Amphora copulata*. Peaks of *Encyonema yellowstonianum* and *Pseudostaurosiropsis* sp., both colonial tube-forming taxa, suggest periods of enhanced turbidity (Krammer, 1997; Ciniglia et al., 2007). *Botryococcus* and *Pediastrum* both occur in this interval, suggesting improved limnic conditions for *Pediastrum* growth.

In summary, during the increasingly cool, wetter summers of the middle Holocene, *Pinus contorta* forest at Goose Lake continued to resemble that of other sites on the Yellowstone Plateau, with increasingly closed or extensive *Pinus contorta* forest and greater fire activity. Geochemical and limnobiotic proxies indicate a sustained thermal influence at Goose Lake, and the diatom data suggest shifts in lake level and enhanced turbidity.

Late Holocene, modern Lower Geyser Basin (GOS3, 3800 cal yr BP–present)

AP:NAP values from Cygnet Lake and Loon Lake suggest continued forest expansion on the Yellowstone Plateau (Whitlock, 1993; Whitlock et al., 1995). At Yellowstone Lake, AP:NAP values remain stable, suggesting little change in forest cover at a regional scale (Theriot et al., 2006). In contrast, the forest at Goose Lake became more open or restricted, as evidenced by decreased AP:NAP values (Fig. 7) resulting from an increase in *Artemisia*, Poaceae, and Amaranthaceae percentages (Fig. 5). This shift likely marks the establishment of modern, open vegetation in LGB. *Artemisia* and Amaranthaceae are not abundant in LGB today and the pollen may have come from steppe vegetation in other parts of Yellowstone National Park, or the Snake River Plain, Idaho, which lies upwind to the west. Both *Artemisia* and Amaranthaceae are prolific pollen producers and long-distance transport from low elevation, semiarid regions has been well documented in pollen studies from the region (Fall, 1992; Whitlock, 1993; Iglesias et al., 2018). Steady but low amounts of *Alnus*, *Betula*, and *Salix* pollen in the late Holocene suggest the presence of riparian areas and wet meadows near Goose Lake (Fig. 5). Charcoal levels at Cygnet Lake indicate increasing fire activity and infrequent, large fire episodes (Fig. 7). In contrast, fire activity declined at Goose Lake, suggesting a more open landscape with little fuel biomass. Fire episodes, evidenced by charcoal peaks, were also less frequent than before at Goose Lake (Fig. 5).

The late Holocene diatom assemblage at Goose Lake differs from that of previous periods, and suggests that the water column was well-mixed with relatively low conductivity. The dominant taxa were *Stephanodiscus minutulus*, *Pinnularia microstauron*, and *Stauroneis americana*. *Stephanodiscus minutulus* is a planktic, high-phosphorous specialist with low nitrogen and silica requirements that blooms in early spring during isothermal mixing (Lynn et al., 2000; Interlandi et al., 2003; Theriot et al., 2006). *P. microstauron* is a benthic species that favors oligotrophic, oxygen-rich waters with low conductivity (Krammer, 2000). *Stauroneis americana* is benthic, preferring wetlands with low to moderate conductivity (Vijver et al., 2005). *Pediastrum* dominated the coccal algae assemblage at Goose Lake in this interval, probably growing along the shallow margins of the lake despite oligotrophic to mesotrophic conditions.

In summary, we suggest an abrupt reorganization of hydrothermal activity in LGB at ca. 3800 cal yr BP explains the pollen and diatom records at Goose Lake (Fig. 7). The Goose Lake pollen record diverges from other Yellowstone Plateau records by showing evidence of more open or limited forest during the late Holocene at a time when forests were becoming more closed or extensive elsewhere in the region. The presence of diatom taxa that previously thrived in warm, thermally influenced waters declined, and the *Botryococcus*-dominated coccal algae assemblage was almost fully replaced by *Pediastrum*. We hypothesize that the development of open vegetation and changes in limnobiota mark the creation of the modern, broad, thermal flat in LGB. This change was contemporaneous with the cessation of hydrothermal activity at Goose Lake.

Potential mechanisms of geo-ecological change ca. 3800 cal yr BP

The shift in hydrothermal activity away from the lake and synchronous creation of broad thermal flats at ca. 3800 yr BP seem a likely explanation for the abiotic and biotic changes registered at Goose Lake, but there is no independent evidence to corroborate this reconstruction. LGB thermal features have not been directly dated, and organic material entombed in siliceous sinter deposits in Upper Geyser Basin ~6 km south of LGB either do not date beyond the past thousand years (Marler, 1956; Hurwitz

https://doi.org/10.1017/qua.2021.42 Published online by Cambridge University Press

et al., 2020), or are unreliable (Lowenstern et al., 2016; but see Churchill et al., 2020).

The shift in hydrothermal activity at 3800 yr BP may have been triggered by changes in geology or climate. Earthquakes (Miller, 1968; Marler and White, 1975; Pitt and Hutchinson, 1982) and ground deformation (Vaughan et al., 2020) are known to abruptly alter hydrothermal activity, and these events have probably affected LGB hydrothermal activity throughout the Holocene. For comparison, the 1959 Hebgen Lake Earthquake (M 7.1, epicenter ~40 km from the Yellowstone Plateau's western thermal areas) altered the activity of many existing thermal features (Marler and White, 1975) and caused new soil heating in the vicinity of Rush Lake in LGB, destroying adjacent forest (Miller, 1968). An earthquake at ca. 3800 cal yr BP could have caused the extinction of the thermal feature(s) at Goose Lake. A significant fault along the western shore of Yellowstone Lake is dated to ca. 3.3 ka based on scarp morphology, radiocarbon dating, and obsidian hydration dating (Locke et al., 1992). Ground uplift related to inflation of the Yellowstone caldera also occurred after ca. 3.8 ka, as inferred from drowned streams and radiocarbon dates at Yellowstone Lake (Pierce et al., 2007a). Either a single or combination of such geological forcings may have been responsible for the hydrothermal shift noted in the Goose Lake record.

Alternatively, climate-driven changes in hydrology may have altered LGB hydrothermal activity at 3800 cal yr BP. For example, Old Faithful Geyser ceased to erupt during a multidecadal drought in the Medieval Climate Anomaly (Hurwitz et al., 2020), so a loss of effective moisture might have altered LGB hydrothermal activity similarly. However, the gradual increase in effective moisture in the late Holocene (Larsen et al., 2020; Chellman et al., 2021) seems inconsistent with abrupt reorganization of the LGB hydrothermal system. Reduced precipitation, however, would have altered the subsurface water supply of LGB, and may have resulted in a reorganization of its hydrothermal activity, including cessation of hydrothermal activity at Goose Lake. This change may have been caused by abrupt drought conditions correlated with the 4.2 ka climate event, a multidecadal period of severe drought in North America (Booth et al., 2005; Lundeen et al., 2013; Carter et al., 2018) and much of the Northern Hemisphere (Railsback et al., 2018). An ice core described from the Beartooth Mountains northeast of Yellowstone National Park indicated a period of anomalous, warmer winter-season temperatures between 4200 cal yr BP and 3800 cal yr BP (Chellman et al., 2021), which may have led to drier conditions in the region. In any case, there has been difficulty in attributing the cause of changes to modern hydrothermal features (e.g., Reed et al., 2021), which cautions against hasty, causal attribution of such changes, particularly in the deep past.

CONCLUSIONS

The Yellowstone Plateau and surrounding mountainous regions have been termed a geo-ecosystem because the ecosystem and other environmental factors are strongly influenced by geological processes, including volcanism, hydrothermal activity, faulting, and tectonic uplift (Pierce et al., 2007b). Paleoecological studies in other regions have noted the legacy of geological processes in shaping vegetation history, either in placing edaphic constraints on vegetation development (Brubaker, 1975; Bernabo, 1981; Briles et al., 2011) or in triggering sudden ecological disturbances (Ogden et al., 2005; Boyd et al., 2005; Long et al., 2014). In most situations, the driving geologic event(s) usually occurred in the deep past (e.g., formation and exhumation of infertile, ultramafic substrate) or had a brief ecological impact (e.g., most volcanic ashfalls). By contrast, the Yellowstone geo-ecosystem remains active, and its ecological history shows a dynamic response to past and ongoing geological processes in concert with climate change. The Holocene record at Goose Lake provides a glimpse into the nature of these interactions at Lower Geyser Basin, with a marked shift in hydrothermal activity during the last ca. 10,300 cal yr that affected the terrestrial and aquatic ecosystems.

Thermal waters discharged directly into Goose Lake prior to ca. 3800 cal yr BP and had little influence on upland vegetation in the basin. In early and middle Holocene, the *Pinus contorta* forest of LGB became increasingly closed and fire activity was generally high, as observed at other sites on the Yellowstone Plateau. Limnic conditions, however, were affected by thermal water discharge, as evidenced by the presence of diatom and coccal algae assemblages adapted to extreme, warm, and potentially somewhat alkaline conditions.

An abrupt reorganization of hydrothermal activity is inferred ca. 3800 cal yr BP, when thermal waters no longer fed directly into Goose Lake. A seismic event may have triggered this shift in basin hydrothermal activity, just as recent earthquakes and uplift have done.

Hydrothermal activity may have become more widespread in LGB ca. 3800 cal yr BP, as inferred from expansion of non-forest vegetation types. The late Holocene vegetation and fire history at Goose Lake diverges from other sites in the region by indicating that the area became more open and sustained few fires. This configuration marks the development of the modern, treeless thermal flat.

Acknowledgments. Field work was conducted under Yellowstone National Park permit YELL-2018-SCI-0009. A. Carlson, R.E. Gresswell, N.E. Kichas, and W.P. Nanavati helped with field work, and J.A. Eggers, B. Hosseini, D.W. Mogk, N. Rieders, and E. Roehm provided laboratory assistance. N.A. Iverson provided unpublished tephrochronological data, V. Iglesias helped with the age-depth model, and S.C. Fritz reviewed the diatom interpretations. S. Hurwitz, J.B. Lowenstern, L.A. Morgan, and an anonymous reviewer provided helpful reviews of the manuscript.

Financial Support. This research was funded by NSF Grant EAR-1515353 to C. Whitlock as part of the HD-YLAKE project and a research fellowship from the Montana Institute on Ecosystems to C.M. Schiller. This work was performed in part at the Montana Nanotechnology Facility, a member of the National Nanotechnology Coordinated Infrastructure (NNCI), which is supported by the NSF Grant ECCS-1542210.

REFERENCES

Arnold, P.G., Sharpe, F.P., 1967. *Summary Report of Lake and Stream Investigations for 1966.* U.S. Fish and Wildlife Service, Yellowstone National Park, WY. Fishery Management Program Lake and Stream Surveys. 102 pp.

Arno, S.F., 1979. Forest Regions of Montana. *USDA Forest Service Research Paper* INT-218, 39 p.

Bahls, L., 2005. Northwest diatoms: a photographic catalogue of species in the Montana Diatom Collection, with ecological optima, associates, and distribution records for the nine northwestern United States. *Northwest Diatoms 2*, The Montana Diatom Collection, Helena. 464 pp.

Bahls, L., 2012. Seven new species in *Navicula* sensu stricto from the Northern Great Plains and Northern Rocky Mountains. *Nova Hedwigia* **141**, 19–38.

Baker, R.G., 1976. Late Quaternary vegetation history of the Yellowstone Lake Basin, Wyoming. *U.S. Geological Survey Professional Paper* 729-E, 1–78.

Bargar, K.E., Beeson, M.H., 1981. Hydrothermal alteration in research drill hole Y-2, Lower Geyser Basin, Yellowstone National Park, Wyoming. *American Mineralogist* **66**, 473–490.

https://doi.org/10.1017/qua.2021.42 Published online by Cambridge University Press

Bartlein, P.J., Anderson, K.H., Anderson, P.M., Edwards, M.E., Mock, C.J., Thompson, R.S., Webb, R.S., Iii, T.W., Whitlock, C., 1998. Paleoclimate simulations for North America over the past 21,000 years: Features of the simulated climate and comparisons with paleoenvironmental data. *Quaternary Science Reviews* **17**, 549–585.

Battarbee, R.W., Jones, V.J., Flower, R.J., Cameron, N.G., 2001. Diatoms. In: Smol, J.P., Birks, J.B., Last, W.M., Bradley, R.S., Alverson, K. (Eds.), *Tracking Environmental Change Using Lake Sediments Volume 3: Terrestrial, Algal, and Siliceous Indicators. Developments in Paleoenvironmental Research 3*, Springer, Dordrecht, The Netherlands, pp. 155–202. https://doi.org/10.1007/0-306-47668-1_8.

Bennett, K.D., Willis, K.J., 2001. Pollen. In: Smol, J.P., Birks, J.B., Last, W.M., Bradley, R.S., Alverson, K. (Eds.), *Tracking Environmental Change Using Lake Sediments Volume 3: Terrestrial, Algal, and Siliceous Indicators. Developments in Paleoenvironmental Research 3*, Springer, Dordrecht, The Netherlands, pp. 5–32. https://doi.org/10.1007/0-306-47668-1_2.

Bergfeld, D., Lowenstern, J.B., Hunt, A.G., Shanks, W.C.P., Evans, W.C., 2014. Gas and isotope chemistry of thermal features in Yellowstone National Park, Wyoming. *U.S. Geological Survey Scientific Investigations Report* **2011-5012**, 1–28.

Bernabo, J.C., 1981. Quantitative estimates of temperature changes over the last 2700 years in Michigan based on pollen data. *Quaternary Research* **15**, 143–159.

Blaauw, M., Christen, J.A., 2011. Flexible paleoclimate age-depth models using an autoregressive gamma process. *Bayesian Analysis* **6**, 457–474.

Blaauw, M., Christen, J.A., Bennett, K.D., Reimer, P.J., 2018. Double the dates and go for Bayes —Impacts of model choice, dating density and quality on chronologies. *Quaternary Science Reviews* **188**, 58–66.

Booth, R.K., Jackson, S.T., Forman, S.L., Kutzbach, J.E., Bettis, E.A., Kreigs, J., Wright, D.K., 2005. A severe centennial-scale drought in mid-continental North America 4200 years ago and apparent global linkages. *The Holocene* **15**, 321–328.

Boyd, W.E., Lentfer, C.J., Parr, J., 2005. Interactions between human activity, volcanic eruptions and vegetation during the Holocene at Garua and Numundo, West New Britain, PNG. *Quaternary Research* **64**, 384–398.

Briles, C.E., Whitlock, C., Skinner, C.N., Mohr, J., 2011. Holocene forest development and maintenance on different substrates in the Klamath Mountains, northern California, USA. *Ecology* **92**, 590–601.

Brown, S., 2019. *Diatom-inferred records of paleolimnological variability and continental hydrothermal activity in Yellowstone National Park, USA*. PhD dissertation, University of Nebraska, Lincoln, USA.

Brubaker, L.B., 1975. Postglacial forest patterns associated with till and outwash in Northcentral Upper Michigan. *Quaternary Research* **5**, 499–527.

Carter, V.A., Shinker, J.J., Preece, J., 2018. Drought and vegetation change in the central Rocky Mountains and western Great Plains: potential climatic mechanisms associated with megadrought conditions at 4200 cal yr BP. *Climate of the Past* **14**, 1195–1212.

Channing, A., Edwards, D., 2003. Experimental taphonomy: silicification of plants in Yellowstone hot-spring environments. *Transactions of the Royal Society of Edinburgh: Earth Sciences* **94**, 503–521.

Chapman, S.S., Bryce, S.A., Omernik, J.M., Despain, D.G., ZumBerge, J., Conrad, M., 2004. *Ecoregions of Wyoming (Color Poster with Map, Descriptive Text, Summary Tables, and Photographs). 1:1,400,000*. U.S. Geological Survey, Reston, Virginia.

Chellman, N.J., Pederson, G.T., Lee, C.M., McWethy, D.B., Puseman, K., Stone, J.R., Brown, S.R., McConnell, J.R., 2021. High elevation ice patch documents Holocene climate variability in the northern Rocky Mountains. *Quaternary Science Advances* **3**, 100021.

Christen, J.A., Pérez, E.S., 2009. A new robust statistical model for radiocarbon data. *Radiocarbon* **51**, 1047–1059.

Christiansen, R.L., Blank, H.R. Jr., 1974. *Geologic Map of the Madison Junction Quadrangle, Yellowstone National Park, Wyoming. 1:62,500*. U.S. Geological Survey, Reston, Virginia.

Churchill, D.M., Manga, M., Hurwitz, S., Peek, S., Licciardi, J.M., Paces, J.B., 2020. Dating silica sinter (geyserite): A cautionary tale. *Journal of Volcanology and Geothermal Research* **402**, 106991.

Ciniglia, C., Cennamo, P., De Stefano, M., Pinto, G., Caputo, P., Pollio, A., 2007. *Pinnularia obscura* Krasske (Bacillariophyceae, Bacillariophyta) from acidic environments: characterization and comparison with other acid-tolerant *Pinnularia* species. *Fundamental and Applied Limnology* **170**, 29–47.

Despain, D.G., 1990. *Yellowstone Vegetation: Consequences of Environment and History in a Natural Setting*. Robert Rinehart Publishers, Boulder, Colorado. 239 p.

Egan, J., Staff, R., Blackford, J., 2015. A high-precision age estimate of the Holocene Plinian eruption of Mount Mazama, Oregon, USA. *The Holocene* **25**, 1054–1067.

Evans, W.C., Bergfeld, D., McGeehin, J.P., King, J.C., Heasler, H., 2010. Tree-ring ^{14}C links seismic swarm to CO_2 spike at Yellowstone, USA. *Geology* **38**, 1075–1078.

Fall, P.L., 1992. Spatial patterns of atmospheric pollen dispersal in the Colorado Rocky Mountains, USA. *Review of Palaeobotany and Palynology* **74**, 293–313.

Fournier, R.O., 1989. Geochemistry and dynamics of the Yellowstone National Park hydrothermal system. *Annual Review of Earth and Planetary Sciences* **17**, 13–53.

Grimm, E.C., 1987. CONISS: a FORTRAN 77 program for stratigraphically constrained cluster analysis by the method of incremental sum of squares. *Computers & Geosciences* **13**, 13–35.

Hedberg, O., 1946. Pollen morphology in the genus *Polygonum* L. s. lat. and its taxonomical significance. *Svensk Botanisk Tidskrift* **40**, 371–404.

Higuera, P.E., Brubaker, L.B., Anderson, P.M., Hu, F.S., Brown, T.A., 2009. Vegetation mediated the impacts of postglacial climate change on fire regimes in the south-central Brooks Range, Alaska. *Ecological Monographs* **79**, 201–219.

Higuera, P.E., Gavin, D.G., Bartlein, P.J., Hallett, D.J., 2011. Peak detection in sediment–charcoal records: impacts of alternative data analysis methods on fire-history interpretations. *International Journal of Wildland Fire* **19**, 996–1014.

Higuera, P.E., Whitlock, C., Gage, J.A., 2010. Linking tree-ring and sediment-charcoal records to reconstruct fire occurrence and area burned in subalpine forests of Yellowstone National Park, USA. *The Holocene* **21**, 327–341.

Hurwitz, S., King, J.C., Pederson, G.T., Martin, J.T., Damby, D.E., Manga, M., Hungerford, J.D.G., Peek, S., 2020. Yellowstone's Old Faithful Geyser shut down by a severe Thirteenth Century drought. *Geophysical Research Letters* **47**, e2020GL089871.

Hurwitz, S., Lowenstern, J.B., 2014. Dynamics of the Yellowstone hydrothermal system. *Reviews of Geophysics* **52**, 375–411.

Iglesias, V., Whitlock, C., Krause, T.R., Baker, R.G., 2018. Past vegetation dynamics in the Yellowstone region highlight the vulnerability of mountain systems to climate change. *Journal of Biogeography* **45**, 1768–1780.

Interlandi, S.J., Kilham, S.S., Theriot, E.C., 2003. Diatom—chemistry relationships in Yellowstone Lake (Wyoming) sediments: Implications for climatic and aquatic processes research. *Limnology and Oceanography* **48**, 79–92.

Jankovská, V., Komárek, J., 2000. Indicative value of *Pediastrum* and other coccal green algae in palaeoecology. *Folia Geobotanica* **35**, 59–82.

Kapp, R.O., Davis, O.K., King, J.E., 2000. *Ronald O. Kapp's Pollen and Spores*. American Association of Stratigraphic Palynologists Foundation, College Station, Texas. 279 p.

Krammer, K., 1997. Die cymbellioden Diatomeen. Eine Monographie der weltweit bekannten Taxa. Teil 1. Allgemeines und *Encyonema* Part. *Bibliotheca Diatomologica* **36**, 1–382.

Krammer, K., 2000. The genus Pinnularia. In: Lange-Bertalot, H. (Ed.), *Diatoms of Europe, Volume 1. Diatoms of the European Inland Waters and Comparable Habitats*. A.R.G. Gantner Verlag, Ruggell, Liechtenstein.

Kylander, M.E., Ampel, L., Wohlfarth, B., Veres, D., 2011. High-resolution X-ray fluorescence core scanning analysis of Les Echets (France) sedimentary sequence: new insights from chemical proxies. *Journal of Quaternary Science* **26**, 109–117.

Larsen, D.J., Crump, S.E., Blumm, A., 2020. Alpine glacier resilience and Neoglacial fluctuations linked to Holocene snowfall trends in the western United States. *Science Advances* **6**, eabc7661. https://doi.org/10.1126/sciadv.abc7661.

Laskar, J., Robutel, P., Joutel, F., Gastineau, M., Correia, A.C.M., Levrard, B., 2004. A long-term numerical solution for the insolation quantities of the Earth. *Astronomy & Astrophysics* **428**, 261–285.

https://doi.org/10.1017/qua.2021.42 Published online by Cambridge University Press

Licciardi, J.M., Pierce, K.L., 2008. Cosmogenic exposure-age chronologies of Pinedale and Bull Lake glaciations in greater Yellowstone and the Teton Range, USA. *Quaternary Science Reviews* **27**, 814–831.

Licciardi, J.M., Pierce, K.L., 2018. History and dynamics of the Greater Yellowstone Glacial System during the last two glaciations. *Quaternary Science Reviews* **200**, 1–33.

Locke, W.W., Meyer, G.A., Pings, J.C., 1992. Morphology of a postglacial fault scarp across the Yellowstone (Wyoming) caldera margin and its implications. *Bulletin of the Seismological Society of America* **82**, 511–516.

Long, C.J., Power, M.J., Minckley, T.A., Hass, A.L., 2014. The impact of Mt. Mazama tephra deposition on forest vegetation in the Central Cascades, Oregon, USA. *The Holocene* **24**, 503–511.

Lowenstern, J.B., Heasler, H., Smith, R.B., 2003. *Hydrothermal disturbances at the Norris Geyser Basin, Yellowstone National Park (USA) in 2003*. American Geophysical Union Fall Meeting 2003, San Francisco, California, Abstract V31B-05.

Lowenstern, J.B., Hurwitz, S., McGeehin, J.P., 2016. Radiocarbon dating of silica sinter deposits in shallow drill cores from the Upper Geyser Basin, Yellowstone National Park. *Journal of Volcanology and Geothermal Research* **310**, 132–136.

Lundeen, Z., Brunelle, A., Burns, S.J., Polyak, V., Asmerom, Y., 2013. A speleothem record of Holocene paleoclimate from the northern Wasatch Mountains, southeast Idaho, USA. *Quaternary International* **310**, 83–95. https://doi.org/10.1016/j.quaint.2013.03.018.

Lynn, S.G., Kilham, S.S., Kreeger, D.A., Interlandi, S.J., 2000. Effect of nutrient availability on the biochemical and elemental stoichiometry in the freshwater diatom *Stephanodiscus minutulus* (Bacillariophyceae). *Journal of Phycology* **36**, 510–522.

Marler, G.D., 1956. How old is Old Faithful Geyser? *American Journal of Science* **254**, 615–622.

Marler, G.D., White, D.E., 1975. Seismic Geyser and its bearing on the origin and evolution of geysers and hot springs of Yellowstone National Park. *Geological Society of America Bulletin* **86**, 749–759.

Meeinkuirt, W., Sirinawin, W., Angsupanich, S., Polpunthin, P., 2008. Changes in relative abundance of phytoplankton in arsenic contaminated waters at the Ron Phibun district of Nakhon Si Thammarat province, Thailand. *International Journal on Algae* **10**, 141–162.

Miller, C.B., 2020. *Arsenic Mobility in a Changing Northern Climate: Implications for Geochemical Baselines and Long-term Stability of Contaminants in Lake Systems*. PhD Dissertation, Queen's University, Kingston, Ontario, Canada.

Miller, L.D., 1968. *Steaming and Warm Ground in Yellowstone National Park: Their Location, Geophysics, Vegetation and Mapping with Aerial Multispectral Imagery*. PhD Dissertation, The University of Michigan, Ann Arbor, USA.

Millspaugh, S.H., Whitlock, C., Bartlein, P.J., 2000. Variations in fire frequency and climate over the past 17 000 yr in central Yellowstone National Park. *Geology* **28**, 211–214.

Moore, P.D., Webb, J.A., Collinson, M.E., 1991. *Pollen Analysis*. 2nd Edition. Blackwell Scientific Publications, Oxford, UK. 216 p.

Morgan, L.A., Shanks, W.C., Pierce, K.L., 2009. Hydrothermal processes above the Yellowstone magma chamber: large hydrothermal systems and large hydrothermal explosions. *Geological Society of America Special Paper* **459**, 1–95.

Muffler, L.J.P., White, D.E., Truesdell, A.H., 1971. Hydrothermal explosion craters in Yellowstone National Park. *Geological Society of America Bulletin* **82**, 723–740.

Muffler, L.J.P., White, D.E., Truesdell, A.H., Fournier, R.O., 1982. *Geologic Map of Lower Geyser Basin, Yellowstone National Park, Wyoming. 1:24,000*. U.S. Geological Survey Miscellaneous Geologic Investigations I-1373, U.S. Geological Survey, Reston, VA.

Ogden, J., Fordham, R.A., Horrocks, M., Pilkington, S., Serra, R.G., 2005. Long-term dynamics of the long-lived conifer *Libocedrus bidwillii* after a volcanic eruption 2000 years ago. *Journal of Vegetation Science* **6**, 21–330.

Onalo, J.I., Matias-Peralta, H.M., Sunar, N.M., 2014. Growth of freshwater microalga, *Botryococcus* sp. in heavy metal contaminated industrial wastewater. *Journal of Science and Technology* **6**, 29–40.

Parsons, M.L., Dortch, Q., Turner, R.E., Rabalais, N.R., 2006. Reconstructing the development of eutrophication in Louisiana salt marshes. *Limnology and Oceanography* **51** 534–544. https://doi.org/10.4319/lo.2006.51.1_part_2.0534.

Patrick, R.M., Reimer, C.W., 1975. The Diatoms of the United States, exclusive of Alaska and Hawaii, volume 2. *Monographs of The Academy of Natural Sciences of Philadelphia* **13**, 1–213.

Pierce, K.L., Cannon, K.P., Meyer, G.A., Trebesch, M.J., Watts, R.D., 2007a. Postglacial inflation-deflation cycles, tilting, and faulting in the Yellowstone Caldera based on Yellowstone Lake shorelines. In: Morgan, L.A. (Ed.), Integrated geoscience studies in the Greater Yellowstone Area—volcanic, tectonic, and hydrothermal processes in the Yellowstone Geoecosystem. *U.S. Geological Survey Professional Paper* 1717, 127–168.

Pierce, K.L., Despain, D.G., Morgan, L.A., Good, J.M., 2007b, The Yellowstone Hotspot, greater Yellowstone ecosystem, and human geography. In: Morgan, L.A. (Ed.), Integrated geoscience studies in the Greater Yellowstone Area—volcanic, tectonic, and hydrothermal processes in the Yellowstone Geoecosystem. *U.S. Geological Survey Professional Paper* 1717, 1–40.

Pitt, A.M., Hutchinson, R.A., 1982. Hydrothermal changes related to earthquake activity at Mud Volcano, Yellowstone National Park, Wyoming. *Journal of Geophysical Research* **87**, 2762–2766.

Planer-Friedrich, B., Lehr, C., Matschullat, J., Merkel, B.J., Nordstrom, D.K., Sandstrom, M.W., 2006. Speciation of volatile arsenic at geothermal features in Yellowstone National Park. *Geochimica et Cosmochimica Acta* **70**, 2480–2491.

Pniewski, F., Sylwestrzak, Z., 2018. Influence of short periods of increased water temperature on species composition and photosynthetic activity in the Baltic periphyton communities. *Biologia* **73**, 1067–1072.

Podder, M.S., Majumder, C.B., 2016. The use of artificial neural network for modelling of phycoremediation of toxic elements As(III) and As(V) from wastewater using *Botryococcus braunii*. *Spectrochimica Acta Part A: Molecular and Biomolecular Spectroscopy* **155**, 130–145.

Ponader, K.C., Potapova, M.G., 2007. Diatoms from the genus *Achnanthidium* in flowing waters of the Appalachian Mountains (North America): Ecology, distribution and taxonomic notes. *Limnologica* **37**, 227–241.

Potapova, M., Snoeijs, P., 1997. The natural life cycle in wild populations of *Diatoma moniliformis* (Bacillariophyceae) and its disruption in an aberrant environment. *Journal of Phycology* **33**, 924–937.

Quigley, M.A., Vanderploeg, H.A., 1991. Ingestion of live filamentous diatoms by the Great Lakes amphipod, *Diporeia* sp.: a case study of the limited value of gut contents analysis. *Hydrobiologia* **223**, 141–148.

Railsback, L.B., Liang, F., Brook, G.A., Voarintsoa, N.R.G., Sletten, H.R., Marais, E., Hardt, B., Cheng, H., Edwards, R.L., 2018. The timing, two-pulsed nature, and variable climatic expression of the 4.2 ka event: A review and new high-resolution stalagmite data from Namibia. *Quaternary Science Reviews* **186**, 78–90.

Reed, M.H., Munoz-Saez, C., Hajimirza, S., Wu, S.M., Barth, A., Girona, T., Rasht-Behesht, M., *et al.*, 2021. The 2018 reawakening and eruption dynamics of Steamboat Geyser, the world's tallest active geyser. *Proceedings of the National Academy of Sciences of the United States of America* **118**, e2020943118.

Reimer, P.J., Austin, W.E.N., Bard, E., Bayliss, A., Blackwell, P.G., Ramsey, C.B., Butzin, M., *et al.*, 2020. The IntCal20 Northern Hemisphere radiocarbon age calibration curve (0–55 cal kBP). *Radiocarbon* **62**, 725–757.

Reimer, P.J., Bard, E., Bayliss, A., Beck, J.W., Blackwell, P.G., Ramsey, C.B., Buck, C.E., *et al.*, 2013. IntCal13 and Marine13 radiocarbon age calibration curves 0–50,000 years cal BP. *Radiocarbon* **55**, 1869–1887.

Reynolds, C.S., 1980. Phytoplankton assemblages and their periodicity in stratifying lake systems. *Holarctic Ecology* [*Ecography*] **3**, 141–159.

Rodman, A., Shovic, H.F., Thoma, D., 1996. Soils of Yellowstone National Park. Yellowstone Center for Resources, Yellowstone National Park, Wyoming. *YCR-NRSR-96-2*. https://www.nrcs.usda.gov/Internet/FSE_MANUSCRIPTS/wyoming/yellowstoneNP_WY1996/yellnpWY1996.pdf. [accessed February 2021]

Salm, C.R., Saros, J.E., Martin, C.S., Erickson, J.M., 2009. Patterns of seasonal phytoplankton distribution in prairie saline lakes of the northern Great Plains (U.S.A.). *Saline Systems* **5**, 1. https://doi.org/10.1186/1746-1448-5-1.

Saros, J.E., Anderson, N.J., 2015. The ecology of the planktonic diatom *Cyclotella* and its implications for global environmental change studies. *Biological Reviews* **90**, 522–541.

Schiller, C.M., Whitlock, C., Alt, M., Morgan, L.A., 2020. Vegetation responses to Quaternary volcanic and hydrothermal disturbances in the Northern Rocky Mountains and Greater Yellowstone Ecosystem (USA). *Palaeogeography, Palaeoclimatology, Palaeoecology* **559**, 109859.

Schiller, C.M., Whitlock, C., Elder, K.L., Iverson, N.A., Abbott, M.B., 2021. Erroneously old radiocarbon ages from terrestrial pollen concentrates in Yellowstone Lake, Wyoming, USA. *Radiocarbon* **63**, 321–342.

Schnurrenberger, D., Russell, J., Kelts, K., 2003. Classification of lacustrine sediments based on sedimentary components. *Journal of Paleolimnology* **29**, 141–154.

Shanks, W.C., Alt, J., Morgan, L.A., 2007. Geochemistry of sublacustrine hydrothermal deposits in Yellowstone Lake—hydrothermal reactions, stable-isotope systematics, sinter deposition, and spire formation. In: Morgan, L.A. (Ed.), Integrated geoscience studies in the Greater Yellowstone Area—volcanic, tectonic, and hydrothermal processes in the Yellowstone Geoecosystem. *U.S. Geological Survey Professional Paper* 1717, 201–234.

Shaw Chraïbi, V.L., 2016. A Paleolimnological Analysis of the Hierarchy of Environmental Controls on the Resilience of Aquatic Communities in Yellowstone National Park, USA. PhD dissertation, University of Nebraska, Lincoln, USA.

Sheppard, J.S., 1971. *The Influence of Geothermal Temperature Gradients upon Vegetation Patterns in Yellowstone National Park*. PhD dissertation, Colorado State University, Fort Collins, USA.

Smith, B.N., Epstein, S., 1971. Two categories of $^{13}C/^{12}C$ ratios for higher plants. *Plant Physiology* **47**, 380–384.

Spatial Analysis Center, Yellowstone National Park, 2020. Fire Perimeters (from 1881 to 2018) in Yellowstone National Park, Wyoming, Montana, Idaho. Spatial Analysis Center, Yellowstone National Park. https://irma.nps.gov/DataStore/Reference/Profile/2188228 [July 9, 2020].

Spaulding, S.A., Bishop, I.W., Edlund, M.B., Lee, S., Furey, P., Jovanovska, E., Potapova, M., 2020. *Diatoms of North America*. https://diatoms.org [October 8, 2020].

Stauffer, R.E., Thompson, J.M., 1984, Arsenic and antimony in geothermal waters of Yellowstone National Park, Wyoming, USA. *Geochimica et Cosmochimica Acta* **48**, 2547–2561. https://doi.org/10.1016/0016-7037(84)90305-3.

Stout, R.G., Al-Niemi, T.S., 2002. Heat-tolerant flowering plants of active geothermal areas in Yellowstone National Park. *Annals of Botany* **90**, 259–267.

Sturchio, N.C., Pierce, K.L., Murrell, M.T., Sorey, M.L., 1994. Uranium-series ages of travertines and timing of the last glaciation in the northern Yellowstone Area, Wyoming-Montana. *Quaternary Research* **41**, 265–277.

Theriot, E.C., Fritz, S.C., Whitlock, C., Conley, D.J., 2006. Late Quaternary rapid morphological evolution of an endemic diatom in Yellowstone Lake, Wyoming. *Paleobiology* **32**, 38–54.

Vaughan, R.G., Heasler, H., Jaworowski, C., Lowenstern, J.B., Keszthelyi, L.P., 2014. Provisional maps of thermal areas in Yellowstone National Park, based on satellite thermal infrared imaging and field observations. *U.S. Geological Survey Scientific Investigations Report* 2014–5137, 1–32. https://doi.org/10.3133/sir20145137.

Vaughan, R.G., Hungerford, J.D.G., Keller, W., 2020. A newly emerging thermal area in Yellowstone. *Frontiers in Earth Science* **8**, 204. https://doi.org/10.3389/feart.2020.00204.

Vijver, B.V. de, Gremmen, N.J.M., Beyens, L., 2005. The genus *Stauroneis* (Bacillariophyceae) in the Antarctic region. *Journal of Biogeography* **32**, 1791–1798.

Waldrop, H.A., Pierce, K.L., 1975. *Surficial Geologic Map of the Madison Junction Quadrangle, Yellowstone National Park, Wyoming*. 1:62,500. U.S. Geological Survey Miscellaneous Geologic Investigations 1-651. U.S. Geological Survey, Reston, Virginia.

White, D.E., Hutchinson, R.A., Keith, T.E.C., 1988. The geology and remarkable thermal activity of Norris Geyser Basin, Yellowstone National Park, Wyoming. *U.S. Geological Survey Professional Paper* 1456, 1–83.

Whitlock, C., 1993. Postglacial vegetation and climate of Grand Teton and southern Yellowstone National Parks. *Ecological Monographs* **63**, 173–198.

Whitlock, C., Bartlein, P.J., 1993. Spatial variations of Holocene climatic change in the Yellowstone Region. *Quaternary Research* **39**, 231–238.

Whitlock, C., Bartlein, P.J., Van Norman, K.J., 1995. Stability of Holocene climate regimes in the Yellowstone region. *Quaternary Research* **43**, 433–436.

Whitlock, C., Larsen, C., 2001. Charcoal as a fire proxy. In: Smol, J.P., Birks, J.B., Last, W.M., Bradley, R.S., Alverson, K. (Eds.), *Tracking Environmental Change Using Lake Sediments Volume 3: Terrestrial, Algal, and Siliceous Indicators. Developments in Paleoenvironmental Research 3*, Springer, Dordrecht, The Netherlands, pp. 75–97.

Whitlock, C., Millspaugh, S.H., 1996. Testing the assumptions of fire-history studies: an examination of modern charcoal accumulation in Yellowstone National Park, USA. *The Holocene* **6**, 7–15.

Wright, H.E., Mann, D.H., Glaser, P.H., 1984. Piston corers for peat and lake sediments. *Ecology* **65**, 657–659.

https://doi.org/10.1017/qua.2021.42 Published online by Cambridge University Press